Molecular Biology of the Cell
Vol. 21, 1125–1139, March 15, 2010

Vav3-deficient Mice Exhibit a Transient Delay in Cerebellar Development

Celia Quevedo, Vincent Sauzeau,* Mauricio Menacho-Márquez,* Antonio Castro-Castro, and Xosé R. Bustelo

Centro de Investigación del Cáncer and Instituto de Biología Molecular y Celular del Cáncer, Consejo Superior de Investigaciones Científicas, University of Salamanca, Campus Unamuno, E-37007 Salamanca, Spain

Submitted April 10, 2009; Revised November 20, 2009; Accepted January 13, 2010
Monitoring Editor: J. Silvio Gutkind

Vav3 is a guanosine diphosphate/guanosine triphosphate exchange factor for Rho/Rac GTPases that has been involved in functions related to the hematopoietic system, bone formation, cardiovascular regulation, angiogenesis, and axon guidance. We report here that Vav3 is expressed at high levels in Purkinje and granule cells, suggesting additional roles for this protein in the cerebellum. Consistent with this hypothesis, we demonstrate using Vav3-deficient mice that this protein contributes to Purkinje cell dendritogenesis, the survival of granule cells of the internal granular layer, the timely migration of granule cells of the external granular layer, and to the formation of the cerebellar intercrural fissure. With the exception of the latter defect, the dysfunctions found in *Vav3*$^{-/-}$ mice only occur at well-defined postnatal developmental stages and disappear, or become ameliorated, in older animals. Vav2-deficient mice do not show any of those defects. Using primary neuronal cultures, we show that Vav3 is important for dendrite branching, but not for primary dendritogenesis, in Purkinje and granule cells. Vav3 function in the cerebellum is functionally relevant, because *Vav3*$^{-/-}$ mice show marked motor coordination and gaiting deficiencies in the postnatal period. These results indicate that Vav3 function contributes to the timely developmental progression of the cerebellum.

INTRODUCTION

The Vav family is a group of signal transduction proteins with oncogenic potential that has single representatives in invertebrate species and three members (Vav1, Vav2, and Vav3) in vertebrates (Bustelo, 2000, 2008; Turner and Billadeau, 2002; Bustelo and Couceiro, 2008). The main known function of all these proteins is to work as guanosine diphosphate (GDP)/guanosine triphosphate (GTP) exchange factors (GEFs) for Rho/Rac proteins (Bustelo, 2000, 2008; Turner and Billadeau, 2002; Bustelo and Couceiro, 2008), a family of Ras-related GTPases involved in cytoskeletal regulation, superoxide production, vesicle trafficking, cell proliferation, and many other biological responses (Etienne-Manneville and Hall, 2002; Bustelo *et al*., 2007). This enzyme activity allows the rapid transition of these GTP-binding proteins from the GDP-bound (inactive) to the GTP-bound (active) state (Bustelo, 2000, 2008; Turner and Billadeau, 2002; Bustelo and Couceiro, 2008). A quite idiosyncratic, and evolutionarily conserved property of these GEFs is that their catalytic function is activated upon phosphorylation by upstream tyrosine kinases (Crespo *et al*., 1997; Schuebel *et al*., 1998; Movilla and Bustelo, 1999; Couceiro *et al*., 2005). The structural basis for the phosphorylation-dependent activation of Vav proteins has been identified recently (Aghazadeh *et al*., 2000; Llorca *et al*., 2005). On activation, these proteins assemble several downstream pathways involved in general processes such as cytoskeletal change, cell cycle transitions, and gene expression, as well as more cell type-specific biological processes that include, among others, immune responses to antigens, phagocytosis, production of reactive oxygen species, and axon guidance events (Bustelo, 2000, 2008; Bustelo, 2000, 2008; Bustelo and Couceiro, 2008). In addition to their catalytic activity, there is experimental evidence indicating that Vav proteins may exert adaptor-like functions (Bustelo, 2001; Saveliev and Tybulewicz, 2009).

The analysis of single, double, and triple knockout mice has shed light on the functional redundancy and specificity of the three Vav family members in the mouse. Thus, it has been shown that Vav1, Vav2, and Vav3 act cooperatively in signaling routes involved in the development, maintenance, and/or effector functions of T and B lymphocytes (Fujikawa *et al*., 2003), as well as in effector functions of platelets (Pearce *et al*., 2004; Pearce *et al*., 2007), neutrophils (Gakidis *et al*., 2004; Miletic *et al*., 2007), macrophages (Hall *et al*., 2006; Miletic *et al*., 2007), and natural killer cells (Cella *et al*., 2004). It has been also shown that Vav2 and Vav3 work together in neurons and endothelial cells to ensure proper axon guidance and angiogenic responses, respectively. These two functions have been linked to the signal transduction pathways regulated by tyrosine kinase receptors of the Eph family (Cowan *et al*., 2005; Hunter *et al*., 2006). In contrast to this functional redundancy, recent data have revealed that Vav family proteins exert specific and nonoverlapping functions in vivo. For example, Vav3-deficient mice, but not *Vav1*$^{-/-}$ or *Vav2*$^{-/-}$ mice, develop massive bones due to defective maturation and signaling of osteoclasts (Faccio *et al*., 2005). *Vav3*$^{-/-}$ mice also develop tachycardia, a renin/angiotensin II-dependent hypertension, cardiovascular remodeling, and renal dysfunctions (Sauzeau *et al*., 2006). These functions have been linked to a hyperactivation of the

This article was published online ahead of print in *MBC in Press* (http://www.molbiolcell.org/cgi/doi/10.1091/mbc.E09–04–0292) on January 20, 2010.

* These authors contributed equally to this work.

Address correspondence to: Xosé R. Bustelo (xbustelo@usal.es).

sympathetic nervous system (Sauzeau *et al*., 2006). Vav2 has been also implicated in blood pressure regulation in vivo (Sauzeau *et al*., 2007). Recently, we have shown that one of the functions of Vav2 in this process is to ensure optimal nitric oxide-dependent signals in vascular smooth muscle cells, the cell type in charge of regulating constriction and relaxation responses of resistance arterioles (Sauzeau *et al*., 2010). Together, these results indicate that Vav proteins, although working together in some biological settings, fulfill specific tasks per se. Such specificity may arise from differential expression patterns and/or by the engagement of unique, tissue-specific downstream elements. An example of the latter possibility is the observation that Vav1, but not Vav2 or Vav3, stimulates the nuclear factor of activated T cells in T lymphocytes (Doody *et al*., 2000; Moores *et al*., 2000; Tartare-Deckert *et al*., 2001). The wide expression pattern of *Vav2* and *Vav3* indicates that they may play additional functions in vivo. In this regard, expression studies have shown that Vav3 is highly expressed in the cerebellum (Movilla and Bustelo, 1999; see also the Allen Brain Atlas at http://mouse.brain-map.org), an organ that plays important roles in sensory perception, motor learning, motor coordination, and cognitive functions (Salman, 2002; Saab and Willis, 2003). To address whether Vav3 plays a role in this tissue, we have analyzed in this work the histological and functional status of the cerebellum in Vav3-deficient mice.

MATERIALS AND METHODS

Animals

Vav3$^{-/-}$ and *Vav2*$^{-/-}$ mice have been described previously (Doody *et al*., 2001; Sauzeau *et al*., 2006, 2007). Animal care and work protocols were approved and carried out according to the regulations set forth by the Animal Research and Welfare committees of the University of Salamanca and Consejo Superior de Investigaciones Cientificas.

Antibodies and Pharmacological Reagents

The rabbit polyclonal antibody to the Vav3 acidic region has been described previously (Movilla and Bustelo, 1999). Antibodies to calbindin were obtained from Swant. Antibodies to Trk family members phosphorylated on residue Y490, to cleaved caspase 3, to phospho-extracellular signal-regulated kinase (Erk), to Erk, and to phospho-Akt were all obtained from Cell Signaling Technology (Danvers, MA). The antibody to Ki67 was purchased from Thermo Fisher Scientific (Waltham, MA). Antibodies to synaptophysin, to GAT1 and to GAD67 were obtained from Millipore Bioscience Research Reagents (Temecula, CA). The mouse monoclonal antibodies (mAbs) to α-tubulin and microtubule-associated protein (MAP)2 were from EMD Biosciences/Oncogene (San Diego, CA) and Sigma-Aldrich (St. Louis, MO), respectively. The mouse mAb to vinculin was from Calbiochem (San Diego, CA). Mouse monoclonal antibodies to Bassoon were purchased in Assay Designs (Ann Arbor, MI). Anti-glial fibrillary acidic protein (GFAP) primary and horseradish peroxidase-conjugated secondary antibodies were obtained from Dako North America (Carpinteria, CA). Cyanine (Cy)3- and Cy2-labeled secondary antibodies were from Jackson ImmunoResearch Laboratories (West Grove, PA). The neurotrophins brain-derived neurotrophic factor (BDNF), neurotrophin (NT)3 and NT4 were obtained from PeproTech (Rocky Hill, NJ).

Immunohistochemistry

In paraffin-embedded sections, cerebella obtained from mice of the indicated genotypes were fixed with 4% paraformaldehyde in phosphate-buffered saline solution (PBS), embedded in paraffin, and cut in 2- to 3-μm sagittal sections. Experiments were done using sections corresponding to the central vermis. In frozen sections, cerebella were cryoprotected by stepwise immersions in 15–30% sucrose–PBS solutions, embedded in Tissue-Tek OCT (Sakura Finetek Europe, Zoeterwoude, The Netherlands), and stored frozen at −70°C. Tissue blocks were then cut sagittally in 16-μm-thick sections using a cryostat. Sections were air-dried for 1 h, rinsed in PBS, blocked and permeabilized with 10% bovine serum albumin (BSA; Sigma-Aldrich) and 0.3% Triton X-100 in PBS for 1 h, and incubated with primary antibodies (diluted in 5% BSA in PBS) overnight at 4°C. After washes in PBS, sections were incubated with the secondary antibody (diluted in PBS), washed, and mounted for immunofluorescence microscopy analysis. To detect spines, we performed anti-calbinin staining with free-floating sections (Rico *et al*., 2002). To this end, animals were anesthetized and perfused serially with PBS, 4% paraformaldehyde in PBS, and several steps of sucrose–PBS solutions (15–30%). Then, 20-μm sections were cut in a sliding microtome. Free-floating sections were preincubated with a PBS solution containing 5% BSA and 0.3% Triton X-100 for 1 h at room temperature and then incubated for 2–3 d at 4°C with anti-calbindin antibodies in PBS supplemented with 1% BSA and 0.3% Triton X-100. Sections were rinsed and incubated with the secondary antibody in the same solution that the primary antibodies. Sections were mounted and analyzed by confocal microscopy using a TSC SP5 system (Leica, Wetzlar, Germany).

Reverse Transcription-Polymerase Chain Reaction (RT-PCR)

Total RNAs were extracted using the RNeasy mini kit (QIAGEN, Hilden, Germany). RT-PCRs were carried out using the iScript one-step RT-PCR kit (Bio-Rad Laboratories, Hercules, CA) and an iCycler apparatus (Bio-Rad Laboratories). Primers for the amplification of the mouse *Vav3* cDNA were 5′-ATG GAG CCG TGG AAG CAG TG-3′ (forward) and 5′-TCC GCC TTC ATC AAG TCT TC-3′ (reverse). Primers for *Shh*, *Astn1*, and *Pax6* transcripts were 5′-GCA TTC CTC TCC TGC TAT GC-3′ (*Shh*, forward), 5′-GTG GCG GTT ACA AAG CAA AT-3′ (*Shh*, reverse), 5′-CCC TGC TGA GCC AGT TCT AC-3′ (*Astn1*, forward), 5′-CCC TGA ACA CCA GAG AGA GC-3′ (*Astn1*, reverse), 5′-AAC AAC CTG CCT ATG CAA CC-3′ (*Pax6*, forward), and 5′-ACT TGG ACG GGA ACT GAC AC-3′ (*Pax6*, reverse). Primers for mouse *Vav2* cDNA were 5′-AAG CCT TTG ACC TTC CAG-3′ (forward) and 5′-GTG TAA TCG ATC TCC CGG GAT-3′ (reverse). The expression levels of mouse *P36b4* mRNA in each RT-PCR sample were used as internal control using oligonucleotide primers 5′-GTG TTT GAC AAC GGC AGC ATT-3′ (forward) and 5′-TTG ATG ATG GAG TGT GGC ACC-3′ (reverse).

Quantitation of Bassoon Signals

OCT sections from P6 cerebella of mice of the indicated genotypes were stained as indicated above, and the Bassoon-specific pixels present in four independent regions of the molecular layer of each slide were quantified using LAS software (Leica).

Golgi Staining of Cerebellar Neurons

To this end, cerebella were frozen in liquid nitrogen, cut in 60-μm-thick sections using a cryostat, and subjected to Golgi staining using the FD Rapid GolgiStain kit (FD Neurotechnologies, Ellicott City, MD) according to the manufacturer's instructions.

Quantification of Layer Thickness and Granular Cell Number

Sagittal sections from the central vermis of cerebella from postnatal day (P)6 and P10 mice of the indicated genotypes were obtained as indicated above, stained with hematoxylin (Sigma-Aldrich), and the thickness of the external granule layers (EGLs) of all cerebellar lobules was measured by drawing a line approximately every 150 μm to calculate the mean of the thickness per lobule. To determine the number of granular cells, the number of nuclei present in a defined area of 4000–5000 μm^2 of the IGL was counted at least in three different areas of the same lobule. We measured the two parameters in six nonconsecutive sections per cerebellum using the ImageJ software (National Institutes of Health; http://rsb.info.nih.gov/ij/).

Quantitation of the Migration of External Cell Layer Granule Cells

To estimate the number of granule cells migrating from the external to the internal granular layer, we counted de visu the number of cells displaying the characteristic "tear drop" shape present in the molecular cell layers of all cerebellar lobules (Adams *et al*., 2002; Chen *et al*., 2005). To this end, we used hematoxylin-eosin stained cerebellar vermis obtained from two P6 wild-type mice and two P6 Vav3-deficient mice.

Quantification of Dying Cells

Dying cells were visualized in P6 sagittal sections by immunohistochemistry with an anti–activated–caspase 3 antibody, as described above. We counted the number of positive cells present in the EGL and the internal granule layer (IGL) in at least eight nonconsecutive sections per cerebellum.

Immunoblot Analysis

E17.5 cerebella and granular cell cultures at division 4 and 5 were disrupted in lysis buffer (20 mM Tris-HCl pH 7.4, 150 mM NaCl, 1% Nonidet-P40, 1 mM phenylmethylsulfonyl fluoride, 1 mM dithiothreitol, 50 mM NaF, 0.2 mM sodium orthovanadate, and the Complete protease inhibitor cocktail [Roche Molecular Biochemicals]). After elimination of cell debris by centrifugation of extracts at 12,000 rpm for 10 min, cell extracts were fractionated electrophoretically, transferred onto nitrocellulose filters using an iBlot dry blotting apparatus (Invitrogen, Carlsbad, CA), and subjected to immunoblot analysis with the indicated antibodies. Immunoreactive bands were developed using an enhanced chemiluminescence system (Pierce Chemical, Rockford, IL).

Densitometry of immunoreactive bands was carried out using the ImageJ software (National Institutes of Health, Bethesda, MD).

Determination of BDNF Concentration

To measure BDNF content in whole cerebella, tissues from P10 animals of the indicated genotypes coming from the same litter were disrupted in lysis buffer. Cellular extracts were cleared by centrifugation and concentrated in an Amicon device (Millipore, Billerica, MA), to a final volume of 200 μl. The protein concentration estimated using a Bradford assay (Bio-Rad Laboratories), and the BDNF levels were determined with the BDNF E_{max} Immunoassay system (Promega, Madison, WI). To measure the BDNF secreted by granular cells, neuronal cultures (divisions 6–7) were depleted for B27 and KCl for 1 h and treated with either 25 mM KCl or 50 ng/ml NT4. Medium was collected after the treatment at the indicated times, and the BDNF concentration at each time point analyzed as described above.

Purkinje Cell Cultures

Cerebella were obtained from newborn mouse pups and transferred onto ice-cold Ca^{2+}/Mg^{2+}-free Hanks' balanced salt solution (Sigma-Aldrich) containing 10 mg/ml gentamicin (Invitrogen). After removal of meninges, cerebella were washed in Ca^{2+}/Mg^{2+}-free HBSS and incubated in 2 ml of a 0.1% trypsin (Invitrogen) solution in Ca^{2+}/Mg^{2+}-free HBSS for 10 min at 35°C. After two washes with Ca^{2+}/Mg^{2+}-free HBSS, cerebella were dissociated using pressure with a Pasteur pipette in 1 ml of Ca^{2+}/Mg^{2+}-free HBSS containing 0.05% DNaseI (Invitrogen) and 12 mM $MgSO_4$ (Sigma-Aldrich). Dissociated tissue suspensions were centrifuged at 1200 rpm for 5 min, and cell pellets were resuspended in 1.5 ml of DMEM/Nutrient Mixture F-12 (Invitrogen) supplemented with 10% fetal bovine serum (Invitrogen). To eliminate nonneuronal cells, the cell suspension was plated onto poly-L-ornithine (Sigma-Aldrich)–coated dishes and incubated at 37°C in 5% CO_2, 95% air for 30 min. Supernatants were collected, and cells were seeded at 5×10^6 cells/ml in serum-free DMEM/F-12 medium containing 100 mM putrescine (Invitrogen), 30 nM sodium selenite (Sigma-Aldrich), 3.9 mM L-glutamine (Invitrogen), 10 mM gentamicin, 4 mM progesterone (Invitrogen), 2 mg/ml insulin (Invitrogen), 20 mg/ml transferrin (Invitrogen), and 0.5 mg/ml tri-iodothyronine (Sigma-Aldrich). Cultures were incubated at 37°C in a 5% CO_2, 95% atmosphere. At 5, 9, and 16 d in vitro, half of the medium was replaced with serum-free culture medium containing 4 mM cytosine arabinoside (Invitrogen). At the end of cultures, cells were fixed and Purkinje cells identified by immunostaining with anti-calbindin antibodies as indicated above.

Granule Cell Cultures and Transfections

Brains from P6–P7 mice were dissected, the cerebellum were excised out, and the overlying meninges and blood vessels were removed in HBSS. Clean cerebella were cut in three pieces and incubated for 20 min at 37°C in Earle's balanced salts (Invitrogen) supplemented with 10 U/ml papain (Worthington Biochemicals, Freehold, NJ), 0.11 mg/ml L-cysteine (Sigma-Aldrich), 0.01% DNAse I (Worthington Biochemicals), and 0.5 mM EDTA. Digestion was stopped by adding onto the aforementioned solution a trypsin inhibitor (ovomucoid, 1 mg/ml; Sigma-Aldrich) and BSA (1 mg/ml). After a mild centrifugation at $280 \times g$ for 2 min, cells were resuspended in Neurobasal medium (Invitrogen) containing 2% of B27 supplement (Invitrogen), 25 mM KCl, penicillin-streptomycin (Invitrogen), and 500 μM L-glutamine. To obtain single-cell suspensions, cells were disrupted with a blue tip and filtered using a 70-μm nylon cell strainer (BD Biosciences, San Jose, CA). After centrifugation for 5 min at $280 \times g$, dispersed neurons were plated onto poly-D-lysine (Sigma-Aldrich)–coated dishes at a density of 5×10^5 cells/cm^2. Cultures were maintained at 37°C in a 5% CO_2-humidified incubator, replacing half of the medium with fresh medium every 2 d. To study dendritic development, neurons were transfected immediately after dissociation with either 1 μg of the retroviral vector pcDH1-MCS1-EF1-CoGFP (System Biosciences, Mountain View, CA) or 6 μg of the same plasmid containing the human *Vav3* cDNA (pCQS1) using a Nucleofactor (Amaxa Biosystems, Gaithersburg, MD). Cell cultures were fixed 4 d later with 4% paraformaldehyde. Measurements of the length of dendrites were carried out in 50 randomly selected, green fluorescent protein (GFP)-positive neurons per condition. At this time of development, dendrites were clearly shorter than axons, so no specific staining was carried out to differentiate between those two neuronal structures.

Behavioral Analysis

Motor coordination tests were performed using an accelerating Rotarod apparatus. The rod unit consisted of a rotating spindle placed above a platform containing plates that stop a LCD timer recording the latencies to fall off the Rotarod. Animals were placed on the plastic tube perpendicular to the axis of rotation starting at 0 rpm. The rod unit was then accelerated to achieve a final speed of 60 rpm/min after 300 s. Latency to fall was recorded and used for data analysis. This protocol was repeated for 5 d with the same mice. Gait analyses were conducted using a 120-cm-long, 9-cm-wide runway platform with 30-cm-high walls on both sides and the starting end. White paper was placed along the bottom of the runway platform. Mice were trained to run down the runway the day before the testing day. Before analysis, the feet of mice were painted using nontoxic acrylic red (forepaws) and blue (hind paws) paint. Footprints were analyzed for stride, stride length, and linear axis.

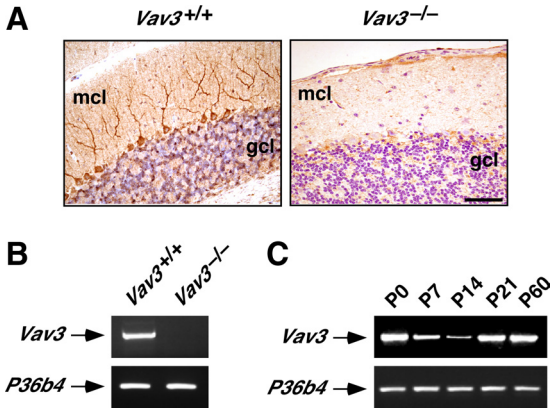

Figure 1. Vav3 is expressed in Purkinje and granular cells of the mouse cerebellum. (A) Anti-Vav3 immunohistochemical analysis of sagittal cerebellar sections obtained from wild-type (left) and *Vav3*$^{-/-}$ (right) mice. mcl, molecular cell layer; gcl, granular cell layer. Bar, 50 μm. Detection of Vav3 immunoreactivity is observed in sections from wild-type animals in both Purkinje cells and in scattered areas of the granular cell layer. (B) Total RNA samples obtained from wild type and *Vav3*$^{-/-}$ granular cell cultures were subjected to RT-PCR analysis using oligonucleotide primers specific for the mouse *Vav3* cDNA (top). As control, aliquots of the same RNAs were amplified using oligonucleotide primers specific for the mouse *P36b4* cDNA (bottom). Final PCR products were separated electrophoretically in agarose gels and photographed. (C) Total RNAs obtained from the cerebella of wild-type mice at the indicated postnatal (P) stages were subjected to RT-PCR analysis using oligonucleotide primers for the mouse *Vav3* (top) and *P36b4* (bottom) cDNAs and processed as indicated above. These results of this figure show that Vav3 is expressed at different levels in the cerebellum in a developmental-dependent manner (C). Furthermore, Vav3 is expressed in this tissue at least in Purkinje (A) and granule cells (B).

Statistical Analysis

Statistical analyses were performed using the *t* test for paired and unpaired data versus control values. Values are given as mean ± SEM.

RESULTS

Expression of Vav3 in Mouse Cerebellum

Previous Northern blot analysis indicated that the human *VAV3* gene is expressed in the cerebellum (Movilla and Bustelo, 1999). Furthermore, the Allen Brain Atlas (http://mouse.brain-map.org) also records high levels of expression of the mouse *Vav3* gene, but not of *Vav1* or *Vav2* genes, in the granular cell layer of the cerebellum. To confirm and expand the expression pattern of that gene in this tissue, we performed immunohistochemical experiments using a home-made, Vav3-specific rabbit polyclonal antibody (Movilla and Bustelo, 1999). These analyses indicated high levels of Vav3 in Purkinje cells and in cells located in the granular cell layer of the cerebellum (Figure 1A, left). In Purkinje cells, Vav3 protein was detected both in the cytoplasm of the somas and in dendrites (Figure 1A, left). No expression of Vav3 was detected instead in molecular cell layer cells (Figure 1A, left). This immunoreactivity was specific for Vav3, because the antibody did not detect those signals in cerebellar sections obtained from Vav3-deficient mice (Figure 1A, right). To verify whether the detection of Vav3 signals in the granular cell layer was due to its expression in Purkinje cell axons or in granular cells, we carried out

RT-PCRs using primary granular cells cultured in vitro. As shown in Figure 1B (top), the band specific for the amplified *Vav3* cDNA was detected in the cultures obtained from wild-type cells but not from *Vav3*$^{-/-}$ granular cells. We performed further RT-PCR experiments to analyze the expression kinetics of the *Vav3* mRNA during cerebellar development. We observed that the expression of the *Vav3* transcript peaked at the time of birth (P0) and at the end of cerebellar development (P21 and adulthood). Moreover, we found that the *Vav3* mRNA underwent a sharp decrease during the developmental interval between P7 and P14 (Figure 1C, top). As control, the *P36b4* mRNA showed a constitutive expression pattern in all the developmental stages surveyed in this study (Figure 1C, bottom). These results indicate that the *Vav3* gene is transcribed both in Purkinje and granule cells and that its expression pattern fluctuates during cerebellar development.

Vav3 Is Important for Intercrural Fissure Formation but Not for the Rest of the Cytoarchitectural Plan of the Cerebellum

The expression of Vav3 in cerebellum led us to investigate whether the Vav3 deficiency could induce defects in the development, structure, or functional status of this organ. Histological analysis indicated that the size of the cerebella of Vav3-deficient mice was similar to that observed in wild-type controls. Moreover, the Vav3 deficiency did not induce any major defect in the overall cerebellar structure, both at P15 (Figure 2A, top) and in the adult period (Figure 2A, bottom). Consistent with this, we observed a fully mature foliation pattern within the vermis of Vav3-deficient cerebella, including the detection of the characteristic folia that were separated by well-developed fissures (Figure 2A). The only exception was the absence of the intercrural fissure, the invagination of the cerebellum that separates lobule VI from lobule VII. This deficiency was consistently observed in both P15 and adult Vav3-deficient mice (Figure 2A, right, arrows). The overall cytoarchitectural organization of the Vav3-deficient cerebella also seemed wild type-like, as assessed by the identification of well-defined molecular, Purkinje, and granular cell layers (Figure 2A). The distribution and morphology of radial glia cells was also normal, as demonstrated by immunofluorescence experiments with antibodies to GFAP (Figure 2B). Altogether, these results indicate that the Vav3 deficiency does not induce major defects in folia development, laminar structure, or glial scaffold organization. Instead, Vav3 participates in the formation of the intercrural fissure.

Vav3 Is Important for the Proper Dendritic Arborization of Purkinje Cells

Despite the conservation of the overall histological structure of the cerebellum in Vav3-deficient mice, a closer analysis of this tissue indicated significant, time-dependent defects in Purkinje cells. When we visualized those cells using antibodies to calbindin (Christakos *et al.*, 1987), we observed that they displayed aberrant cell morphologies in P6 *Vav3*$^{-/-}$ mice. Thus, although the Purkinje cells were properly aligned in the expected cerebellar layer (Figure 3A, right), they had smaller and poorly branched dendritic trees (Figure 3A, right). Furthermore, we found Purkinje cells containing two or more thin dendritic stems sprouting from the somas that were clearly different from the single primary stem present in wild-type cells at this developmental stage (Figure 3A, bottom on the right). As a consequence of this deficient arborization, the thickness of the molecular layer was significantly reduced in Vav3-deficient cerebella compared with their wild-type counterparts (Figure 3A). Despite these defects, we found that Purkinje cells had normal numbers (data not shown) and were arranged in a wild-type-like laminar distribution in *Vav3*$^{-/-}$ mice independently of the cerebellar lobule analyzed (Figure 3, A and B). Likewise, we could also observe that each Purkinje cell projected axons to the underlying white matter tracks (Supplemental Figure S1), indicating that axogenesis was not impaired in the absence of Vav3 expression. Consistent with this, we found normal levels of calbindin staining in the fastigial deep nucleus (data not shown, but see below; and Supplemental Figure S3), the main target of the GABAergic axons of Purkinje cells located in the anterior lobules of the cerebellum.

Because the developmental period encompassed between P3 and P28 is characterized by the formation of synaptic contacts between the growing Purkinje cell dendrites and parallel and climbing fibers in the molecular cell layer (Sotelo, 2004), we next investigated whether the *Vav3* gene loss could result in defective synapse formation. Using immunolocalization experiments for synaptophysin, a general component of presynaptic vesicles (Buckley, 1994), we detected

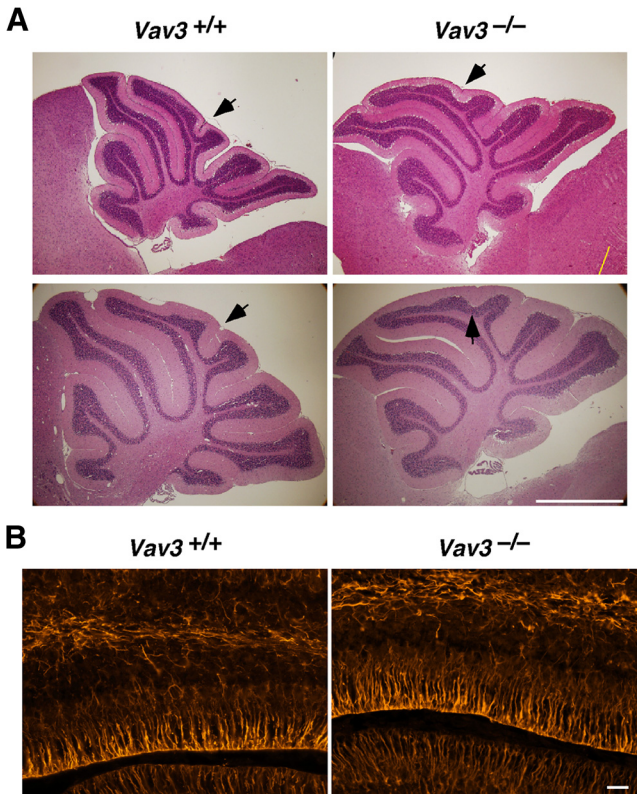

Figure 2. Histological and cytological alterations in cerebella obtained from Vav3-deficient mice. (A) Sagittal cerebellar sections from P15 (top) and adult stages (bottom) obtained from wild-type (left) and Vav3-deficient (right) were stained with hematoxylin and eosin and analyzed by light microscopy. Bar, 1 mm. It is observed a normal structure of the cerebella of Vav3-deficient mice, with the exception of a poorly developed intercrural fissure that separates cerebellar lobules VI and VII (compare areas of the left and right panels that have been pointed out by arrows). (B) Detection by immunofluorescence of the expression of GFAP in sagittal cerebellar sections obtained from P6 wild-type (left) and *Vav3*$^{-/-}$ (right) mice. Pictures show representative images obtained in cerebellar lobule IV. Similar results were obtained in the rest of cerebellar lobules analyzed (data not shown). Bar, 60 μm. No changes in the distribution of GFAP are seen in the cerebella of control and Vav3-deficient mice.

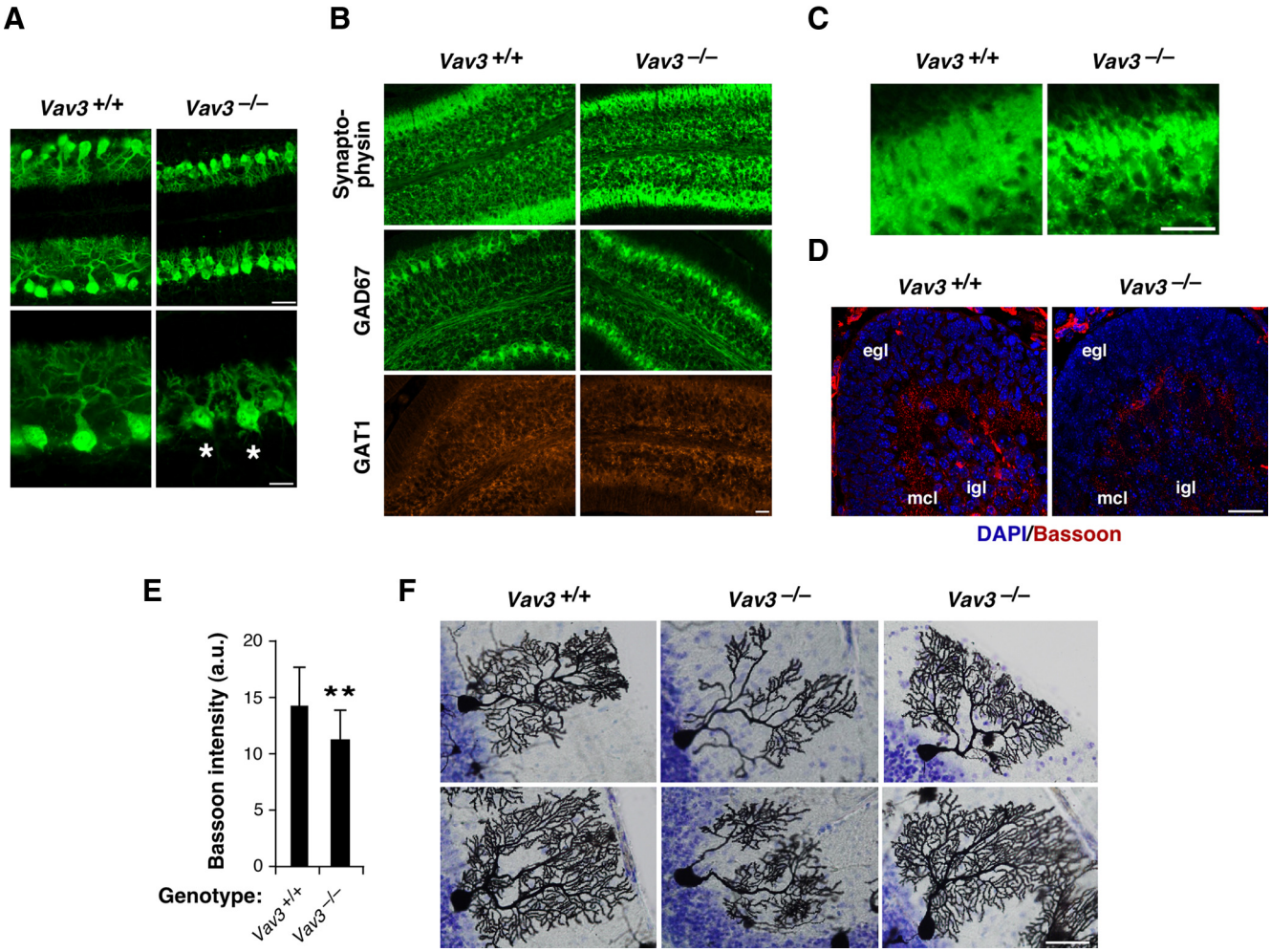

Figure 3. Deficient dendritic arborization of $Vav3^{-/-}$ Purkinje cells. (A) Sagittal cerebellar slices from P6 wild-type (left) and $Vav3^{-/-}$ (right) mice were stained with an anti-calbindin antibody to visualize Purkinje cells. Representative fluorescence images for the lateral part of lobule V and VI are shown in low- (top; bar, 60 μm) and high (bottom; bar, 30 μm)-power views. Signals derived from calbindin are seen in green color in the images. Asterisks label two Purkinje cells with two dendrite main trunks branching out independently from the soma. A clear defect in the arborization of the dendritic tree of Purkinje cells is observed in Vav3-deficient mice. Note also that the thickness of the molecular layer is reduced in those animals (compare top panels). (B and C) Detection by immunofluorescence techniques of the expression of synaptophysin (B, top; for a magnification of those images, see C), GAD67 (B; second row of panels from top), and GAT1 (B; third row of panels from top) in sagittal cerebellar sections obtained from P6 wild-type mice (B and C; left) and $Vav3^{-/-}$ mice (B and C; right). Signals from synaptophysin (B and C) and GAD67 (B) are shown in green. Those from GAT1 are shown in red (B). Pictures show representative images obtained in cerebellar lobule IV. Similar results were obtained in the rest of cerebellar lobules analyzed (data not shown). Bar, 60 μm. (D) Detection by immunofluorescence techniques of the expression of the presynaptic Bassoon marker in cerebellar sections obtained from P6 wild-type mice (left) and Vav3-deficient mice (right). Signals from Bassoon protein are shown in red. Those from the 4,6-diamidino-2-phenylindole counterstaining are shown in blue. Bar, 100 μm. The cerebellar regions corresponding to the external granular cell layer (egl), the molecular cell layer (mcl), and the internal granular cell layer (igl) are indicated. (E) Quantification of Bassoon immunoreactivity in the molecular layer of the cerebella obtained from mice of the indicated genotypes (n = 4 animals). **$p < 0.01$ compared with wild-type controls. a.u., arbitrary units. It is observed that Vav3-deficient mice show lower levels of Bassoon immunoreactivity in their cerebellar molecular layers. (F) Examples of Golgi-stained Purkinje cells present in sections of adult mice cerebella obtained from wild-type mice (left) and Vav3-deficient mice (middle and right). Bar, 50 μm. With the exception of a Purkinje cell shown in the middle bottom panel, the structure of wild-type and Vav3-deficient Purkinje cells is similar (compare rest of panels).

staining of this marker in the molecular and granular cell layers of both $Vav3^{+/+}$ and $Vav3^{-/-}$ cerebella (Figure 3B, top). Despite this, we noticed a different structure of the synaptophysin-positive structures in the Purkinje cell layer, because the structures present in Vav3-deficient mice concentrated in patches near the Purkinje cell somas and showed a less dispersed distribution within the molecular layer than those present in control mice (Figure 3B; but also see an enlarged view of this picture in Figure 3C). Using similar experiments, we found that the presynaptic GABAergic marker GAD67 was also present in $Vav3^{-/-}$ mice, although, as in the case of synaptophysin, the signals were more concentrated in proximal areas to Purkinje cell somas (Figure 3B, middle). Instead, we did not find any significant change in the distribution of GAT1 (Figure 3B, bottom), a marker present in axon terminals of inhibitory, GABAergic cells (basket, stellate, and Golgi cells) of the cerebellum (Morara *et al.*, 1996). Because the above-mentioned proteins gave very strong signals in animals of both genotypes, we looked for an additional marker that could allow us a better

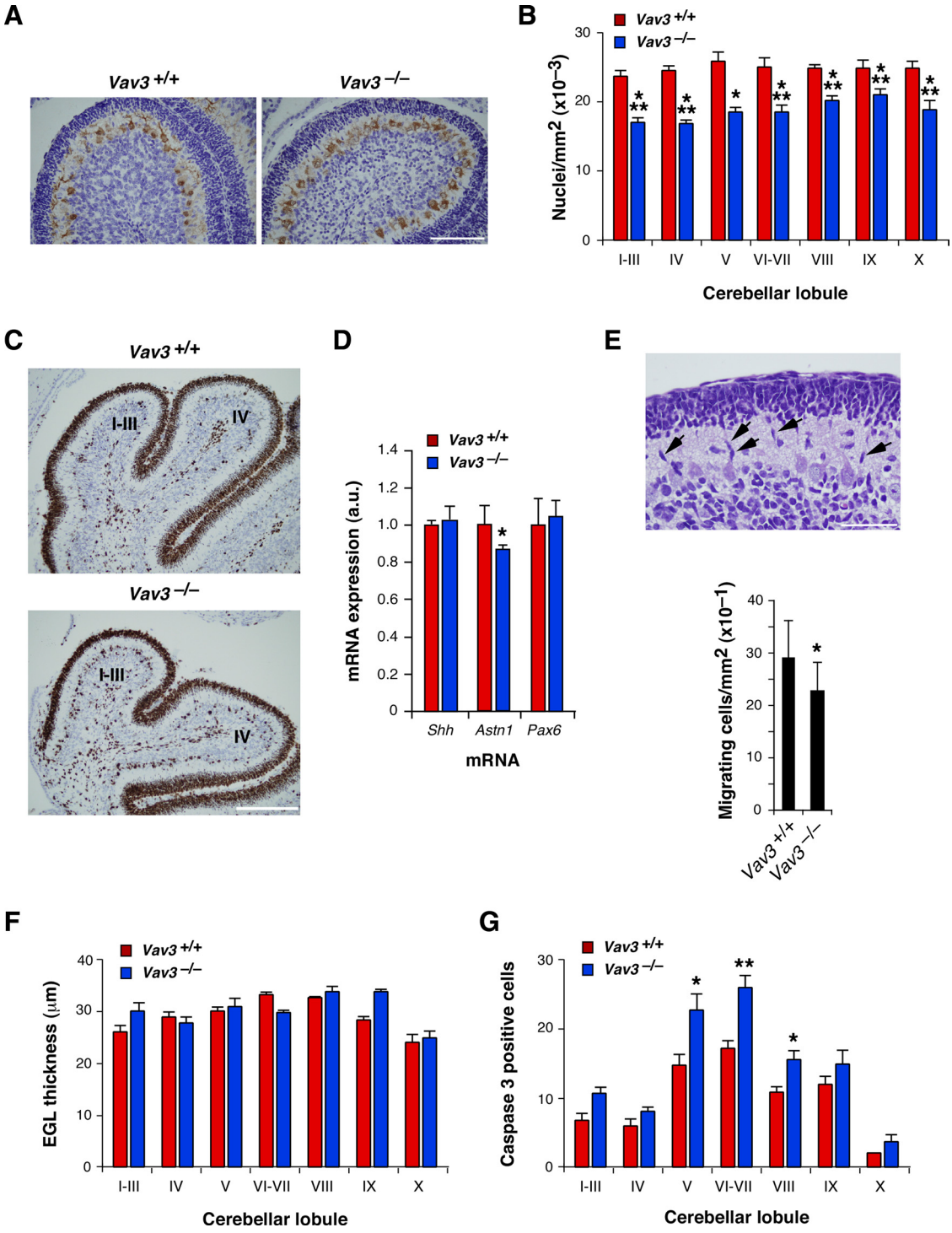

Figure 4. Pleiotropic effects of the *Vav3* proto-oncogene deficiency in cerebellar granular cells. (A) Sagittal sections of P6 cerebella from wild-type mice (left) and *Vav3*$^{-/-}$ mice (right) were immunolabeled with an anti-calbindin antibody to identify Purkinje cells and then stained with hematoxylin. Bar, 100 μm. A reduction in cell density is observed in the IGL from Vav3-deficient mice. (B) Quantification of the cell density (measured as number of nuclei per square millimeter) present in the IGL of the indicated cerebellar lobules of wild-type animals (red bars) and Vav3 knockout animals (blue bars). The histogram shows the mean and the SEM obtained in each cerebellar lobule using experimental data from four different animals and two independent litters per genotype. *$p < 0.05$, **$p < 0.01$, and ***$p < 0.001$ compared with wild-type controls. A statistically significant reduction in the number of cells present in the IGL is observed in *Vav3*$^{-/-}$ mice. (C) Immunohistochemical analysis of Ki67 protein expression in sagittal cerebellar sections from P6 mice from wild-type mice (top) and *Vav3*$^{-/-}$ mice (bottom). Pictures show representative images for lobules I–III and IV. Bar, 200 μm. No significant variations in proliferating cells were observed between control and Vav3 knockout animals. (D) Quantitation by RT-PCR of proliferative (*Shh*) and migratory (*Astn1*, *Pax6*) granule cells in the cerebella of P6 wild-type mice (red bars; n = 3) and Vav3-deficient mice (blue bars; n = 5). *$p < 0.05$ compared with wild-type controls. The graph shows that some migration markers (*Astn1*) are down-modulated in Vav3-deficient mice. Instead, no alterations are found in the expression of the proliferative and migratory *Shh* and *Pax6* markers, respectively. (E) Top, example of "tear drop"-shaped granule cells

visualization of synaptic contacts. To this end, we used antibodies to Bassoon, a 420-kDa protein present in the presynaptic side of active synaptic junctions and that colocalizes with both GABA and Glutamate GluR1 receptors. As shown in Figure 3D, Bassoon-positive signals were detected as discrete points throughout the molecular layer of cerebellar slices from P6 wild-type mice. Such immunoreactivity was slightly, although statistically significant reduced in slices from P6 Vav3-deficient mice (Figure 3, D and E). These results indicate that the Vav3 deficiency leads only to very minor disruptions in the synaptogenesis of Purkinje cells.

To get a developmental perspective of the above-mentioned defects, we studied the cerebella of *Vav3*$^{-/-}$ mice at different developmental stages. We first investigated the Purkinje cell status at embryonic stage (E)17.5, a developmental stage in which those cells are migrating from the germinal layer of the fourth ventricle to their final niche (Sotelo, 2004). Using immunolocalization experiments with anti-calbindin antibodies, we observed that Purkinje cell precursors showed the expected localization in the developing cerebellar plate at this developmental stage regardless of the genotype of the mice analyzed (Supplemental Figure S2A). The total levels of expression of calbindin were also the same in wild-type and Vav3-deficient animals at this stage (Supplemental Figure S2B), further indicating that *Vav3*$^{-/-}$ mice have no major defects in the total number or migration of Purkinje cell progenitors. At P10, we observed a significant rescue of the defects found in the Purkinje cell dendritic trees, although their arborization patterns were still of less complexity than those of wild-type cells. The frequency of Purkinje cells displaying two dendrite stems was significantly reduced (data not shown; but see Figure 5C). At P15, we observed still reduced arborization of Purkinje cells (Supplemental Figure S3) but normal axon projections (Supplemental Figure S3) and innervation of the fastigial nucleus by Purkinje cell axons (Supplemental Figure S3). In addition, the spines of tertiary dendrites present in the mutant mice show densities similar to those found in wild-type mice (Supplemental Figure S3; data not shown). It should be noted, however, that because the dendritic trees are less complex between P6 and P15, the total number of spines is probably reduced at those stages in *Vav3*$^{-/-}$ mice.

In adult mice, a time in which all the cerebellar development has taken place, the use of Golgi staining techniques revealed that some *Vav3*$^{-/-}$ Purkinje cells still had poor arborization and, in some cases, two primary dendrite trunks emanating from the cell body (Figure 3F, middle). However, unlike in the previous developmental stages, the majority of Purkinje cells from 2-month-old *Vav3*$^{-/-}$ animals showed shapes and arborizations very similar to those found in wild-type mice (Figure 3F, compare left and right). As in previous stages, we also found normal spines in the dendrites of Purkinje cells (Figure 3F; and data not shown). These results indicate that the Vav3 deficiency delays the formation of the Purkinje cell dendritic tree during a specific interval of cerebellar development. Instead, Vav3 is not important for the initial development and migration of Purkinje precursors, for axon projections, or for spinogenesis.

Pleiotropic Effects of the Vav3 Gene Deficiency in Granule Cells

The histological analysis of cerebellar sections from P6 animals also revealed that the Vav3 deficiency led to a 20–30% reduction in the cell density of neurons of the IGL of all cerebellar lobules (Figure 4, A and B). At this developmental stage, granule cell precursors proliferate initially in the outer zone of the EGL; exit the cell cycle; differentiate; migrate through the molecular layer and the Purkinje cell layer; and, eventually, stop migrating in their final destination in the IGL. In the process, they establish synaptic contacts with dendrites of Purkinje cells (Altman, 1972a,b,c; Hatten and Heintz, 1995; Sotelo, 2004). Thus, the difference in IGL cell density found in *Vav3*$^{-/-}$ cerebella could potentially be due to reduced proliferation, migration from the EGL to the IGL, and/or survival rates within either the EGL or the IGL. We could not detect any difference in the proliferation rates of EGL-localized *Vav3*$^{-/-}$ cells, as assessed by immunohistological experiments with antibodies to the proliferative marker Ki67 (Figure 4C). Likewise, we did not detect by quantitative RT-PCR experiments significant variations in the expression of *Shh* (Figure 4D), a mitogen for the proliferation of granule cell progenitors (Wechsler-Reya and Scott, 1999). In contrast, we found that the migration of those cells was slightly affected at this stage. Thus, examination of the molecular cell layers revealed that those from Vav3-deficient mice had reduced numbers of "teardrop"-shaped granule cells (Figure 4E). Because cells showing that morphology are linked to migratory behavior (Adams *et al*., 2002; Chen *et al*., 2005), these findings suggest that the migration of these cells are somewhat disrupted in *Vav3*$^{-/-}$ mice. This disruption is rather subtle because, as shown in Figure 4D, quantitative RT-PCR experiments indicated that the expression of some genes associated to granule cell migration does not change significantly (*Pax6*) (Yamasaki *et al*., 2001) or, if it does (*Astn*) (Adams *et al*., 2002), it does so slightly. Likewise, we did not detect any significant increase in the thickness of the EGL (Figure 4F), a parameter that is usually increased when severe defects in granule cell migration are present in mice. Finally, whereas these two mouse strains showed the same total number of caspase-3–positive cells in their EGLs (data not shown), we observed larger numbers of apoptotic cells in the IGLs of cerebellar lobules V, VI–VII, and VIII from Vav3-deficient mice (Figure 4G). A similar tendency, which showed no statistical significance, was also seen in other cerebellar lobules of *Vav3*$^{-/-}$ mice (Figure 4G). These results indicate that the Vav3 deficiency affects the migration of granule cells from the EGL to the IGL and, in addition, the survival of granule cells at the IGL.

Figure 4 (cont). in the molecular layer of a wild type cerebellum. Some migrating cells are shown by arrows. Bar, 50 μm. Bottom, quantitation (measured as number of cells per square millimeter) of the number of migrating granular cells in the molecular layers of wild-type and *Vav3*$^{-/-}$ mice. *$p < 0.05$ compared with wild-type controls. The graph shows that there is a slight, although statistically significant reduction in the number of migrating cells in the cerebella from Vav3-deficient mice. (F) Sagittal sections of P6 wild-type mice (red bars) and *Vav3*$^{-/-}$ mice (blue bars) were stained with hematoxylin and eosin, and the thickness of the EGL was measured in all lobules as described in *Materials and Methods*. Values represent the mean and SEM from two different animals and two different litters for each genotype. No statistically significant variations were observed in the EGL thickness between wild-type and Vav3-deficient mice at the P6 stage. (G) Sagittal cerebellar sections from P6 wild-type mice (red bars) and *Vav3*$^{-/-}$ mice (blue bars) were immunolabeled with an anti-cleaved caspase-3 antibody and the number of apoptotic cells in the IGL quantified de visu. Values represent the mean and SEM of the total number of apoptotic cells relative to de total number of cells present in the IGL. A minimum of four different animals and three different litters for each genotype were analyzed. *$p < 0.05$ and **$p < 0.01$ compared with wild-type controls. A statistically significant increase in the percentage of apoptotic cells was observed in the lobules V, VI–VII, and VIII of 6d-old Vav3-deficient mice.

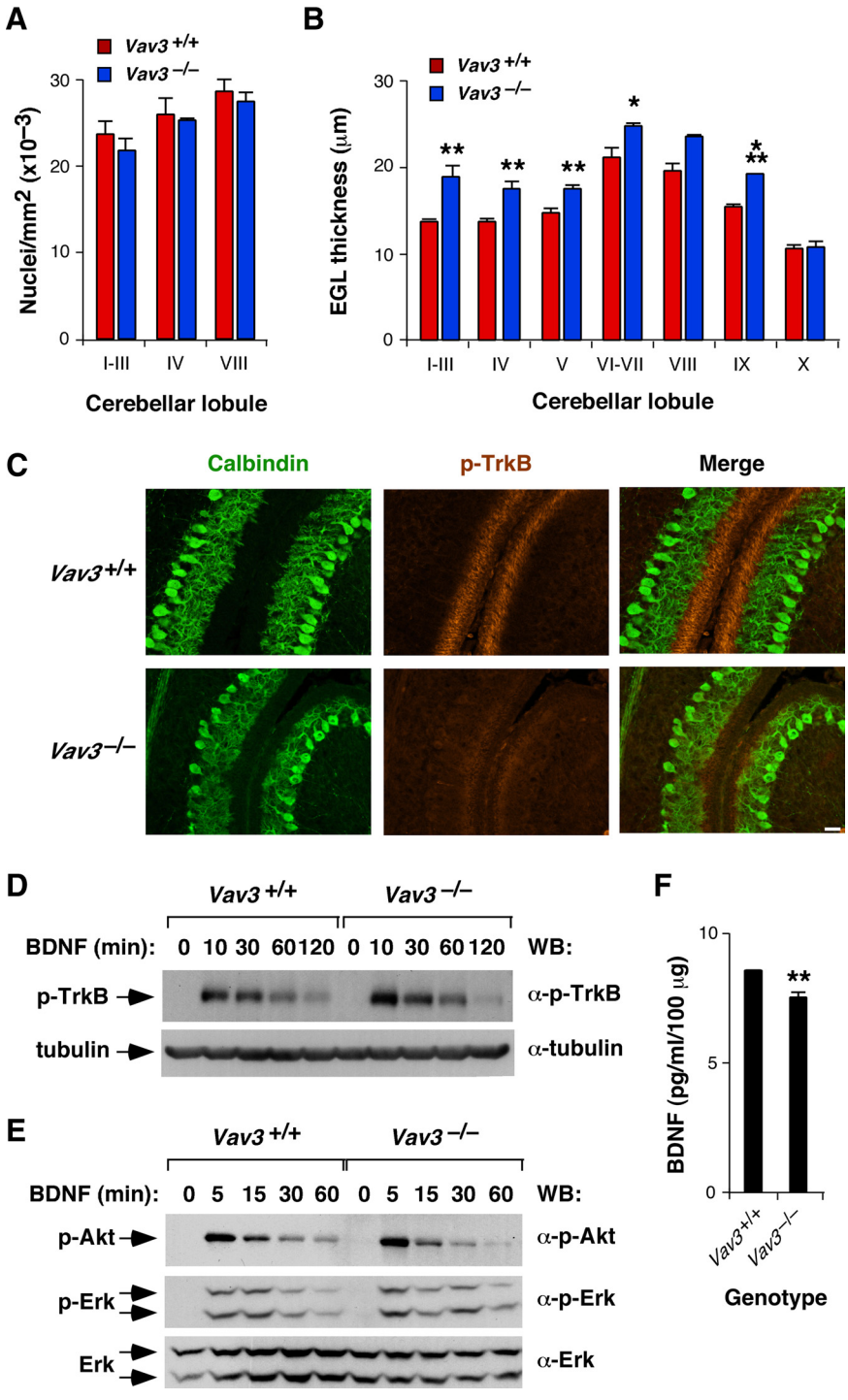

Figure 5. P10 *Vav3*$^{-/-}$ mice show a defect in cerebellar layer formation but not in IGL apoptosis. (A) Quantification of the cell density (measured as number of nuclei per square millimeter) present in the IGL of the indicated cerebellar lobules of P10 wild-type mice (red bars) and Vav3-deficient mice (blue bars). The histogram shows the mean and the SEM obtained in each cerebellar lobule using experimental data from four different animals and two independent litters per genotype. No differences are observed in the cell densities of P10 IGLs from wild-type and Vav3-deficient mice. (B) Sagittal sections obtained from the vermis of P10 wild-type (red bars) and Vav3-deficient (blue bars) animals were stained with hematoxylin and eosin, and the thickness of the EGL measured in all lobules as described in *Materials and Methods*. Values represent the mean and SEM from five different animals coming from two different litters for each genotype. *$p < 0.05$, **$p < 0.01$, and $p < 0.001$ compared with wild-type controls. A statistically significant increase in the thickness of the EGLs of cerebellar lobules I–III, IV, V, VI–VII, and IX is observed in Vav3-deficient animals. (C) Sagittal sections from the vermis of P10 wild-type (top) and *Vav3*$^{-/-}$ (bottom) mice were stained and subjected to immunofluorescence experiments using antibodies to calbindin (left and right) and phospho-panTrk (middle and right). The immunoreactivity obtained with the anti-calbindin and phospho-panTrk antibodies is shown in green and red, respectively. Areas of colocalization are observed in yellow (right). Representative images show part of lobule V and VI. Similar staining patterns were observed throughout all cerebellar cortices analyzed. Bar, 60 μm. Anti-panTrk immunoreactivity was localized around the upper region of the molecular layer that lies beneath the EGL. This is the region were the tips of the extending dendrites of Purkinje cells and the PF terminals extending from granule cells are concentrated. Such staining is reduced in the same areas of Vav3-deficient animals. (D and E) Cellular extracts from wild-type and *Vav3*$^{-/-}$ granule cells stimulated with BDNF for the indicated periods of time were analyzed by Western blot (WB) analysis using antibodies to phospho-TrkB (D, top), α-tubulin (D, bottom), phospho-Akt (E, top), phospho-Erk (E, middle), and Erk (E, bottom) (n = 5). p, phosphorylated. No significant changes in the phosphorylation levels of TrkB (D), Akt (E), and Erk (E) were observed in BDNF-stimulated Vav3-deficient granule cells compared with their wild-type counterparts. (F) Production of BDNF by cerebella obtained from P10 animals (n = 5). **$p < 0.01$ compared with wild-type controls. A statistically significant decrease in BDNF production was observed in the cerebella from Vav3-deficient animals.

The enhanced apoptosis found in Vav3-deficient animals is also developmentally controlled, because we did not observe statistically significant disparities in cell densities between the IGLs of P10 *Vav3*$^{-/-}$ and control animals (Figure 5A). At this developmental stage, the peak of EGL and IGL granule cell programmed cell death has taken place already (Wood *et al.*, 1993; Krueger *et al.*, 1995). During this period, however, the EGL is undergoing a large reduction in its cell layers, evolving from the usual seven- to 10-cell strata thickness typical of the P8 stage to the one to two cell layer state usually observed at P14 (Altman, 1972a; Hatten and Heintz, 1995; Sotelo, 2004). We observed that this process was delayed in Vav3-deficient animals, because their EGLs were 15–36% thicker than those of control animals (Figure 5B). The only exception was lobule X, which showed no significant change in its thickness when compared with wild-type

controls (Figure 5B). This delayed layer formation was rescued at later developmental stages, because we observed no differences in the EGL thickness of P15 wild-type and Vav3-deficient mice (Figure 2A, top; data not shown). The EGL disappeared completely in the adult period in both mouse strains (Figure 2A, bottom; data not shown).

Because the migration of granule cells is mediated by the BDNF neurotrophin and its receptor the tropomyosin receptor kinase (Trk)B tyrosine kinase (Zhou *et al*., 2007), we decided to investigate the status of the BDNF/TrkB signaling route in Vav3-deficient mice. To this end, we stained P10 cerebella from animals of the indicated genotypes with an antibody to autophosphorylated, activated Trk. This antibody recognizes the phosphorylated Y490 residue present in all Trk family members. This site reflects well the activation state of these transmembrane receptors, because its phosphorylation favors the proliferation and survival of cells via the stimulation of the Sos/Ras/Erk and the phosphatidylinositol 3-kinase/Akt routes, respectively (Stephens *et al*., 1994; Segal *et al*., 1996). We observed strong phospho-panTrk immunoreactivity in the EGL of wild-type mice (Figure 5C, top). By contrast, the phospho-panTrk immunoreactivity was significantly weaker in *Vav3*$^{-/-}$ animals (Figure 5C, bottom). This defect was observed in all cerebellar lobules (data not shown). To investigate the cause of the defective activation of TrkB, we first investigated the signaling of BDNF in primary cultures of cerebellar granule cells. We could not detect any abnormal signaling of *Vav3*$^{-/-}$ primary granule cells, because they reacted to BDNF stimulation by inducing normal levels and kinetics of phosphorylation of TrkB and TrkB downstream elements, including Erk and Akt (Figure 5, D and E). Similar results were obtained when these cells were stimulated with KCl or NT3 (data not shown). These results indicate that the low activation levels of TrkB found in *Vav3*$^{-/-}$ P10 EGLs are not due to intrinsic signaling, biosynthetic or recycling defects in the TrkB receptor. Abnormal activation of TrkB can be also mediated by inefficient BDNF synthesis or bioavailability. For example, the loss of calcyphosine 2, a protein involved in neurotrophin release (Sadakata *et al*., 2004), also promotes poor activation levels of TrkB in the EGL (Sadakata *et al*., 2007). When we measured the BDNF concentration in P10 cerebella, we found slightly low amounts of the neurotrophin in the cerebellar extracts obtained from *Vav3*$^{-/-}$ mice (Figure 5F). Because BDNF is produced and secreted by granular cells in the cerebellum (Wetmore *et al*., 1990; Rocamora *et al*., 1993), we next investigated BDNF production in those cells using primary cultures. In contrast to the data obtained in cerebellar tissue extracts, we did not find any statistically significant difference in the secretion of BDNF in cultured wild-type (51.24 $\pm$ 0.47 pg/ml) and *Vav3*$^{-/-}$ (56.32 $\pm$ 1.96 pg/ml) granule cells upon NT4 stimulation for 8 h (n = 3). Similar results were obtained when granule cells were stimulated with KCl for 4 h (4.6 $\pm$ 0.51 pg/ml in wild-type cells vs. 5.671 $\pm$ 0.47 pg/ml in *Vav3* knockout cells). These results indicate that the lower levels of BDNF in tissue extracts derived from *Vav3*$^{-/-}$ mice are not due to intrinsic deficits in the production of the neurotrophin by *Vav3*$^{-/-}$ granule cells, suggesting that they may result instead from the lower numbers of granular cells present in prior stages (i.e., P6).

Vav3 Regulates Dendrite Formation in Purkinje and Granule Cells

Given the defective dendrite arborization found in the developing *Vav3*$^{-/-}$ cerebellum, we decided to investigate this process in more detail using in vitro cultures of both Purkinje and granule cells. We observed that cultured Purkinje cells from Vav3-deficient mice could develop the primary dendrite trunks in vitro and expand them to generate dendritic tree areas similar to those induced in wild-type cells (Figure 6, A and B). However, the *Vav3* gene deficiency induced severe defects in the branching of those dendrite trunks to generate secondary and tertiary dendrites (Figure 6A). As a consequence, the number of branching points per Purkinje cell decreased ~7-fold compared with those formed by wild-type cells (Figure 6B, right). When we analyzed primary granule cell cultures, we observed no gross alterations in the dendrite formation using immunofluorescence techniques (data not shown). However, the analysis of protein extracts from these cells at different divisions in culture (DIV) times indicated that *Vav3*$^{-/-}$ granule cells had a consistent reduction in the levels of MAP2) (Figure 6, C and D). These results were indicative of dendrite dysfunctions in Vav3-deficient granule cells, because MAP2 is an important regulatory protein involved in dendrite morphogenesis (Friedrich and Aszodi, 1991). To verify this possibility, we carried out transient transfections in primary cultures of granule cells using mammalian expression vectors expressing the enhanced green fluorescent protein (EGFP) or coexpressing the EGFP plus a c-Myc–tagged version of wild-type Vav3. After transfection, cells were fixed and examined by immunofluorescence microscopy to identify EGFP-positive cells and quantify their dendritic processes (Figure 6E). These experiments indicated that the overexpression of wild-type Vav3 increased the total dendrite length per cell (596 $\pm$ 176 vs. 406 $\pm$ 178.8 μm of cells expressing EGFP alone), as well as the total number of dendritic branching tips (12 $\pm$ 0.6 vs. 8 $\pm$ 0.5 of cells expressing EGFP alone; Figure 6F). These results indicate that Vav3 affects dendrite branching in both Purkinje and granule cells.

Vav2 Is Also Expressed in the Cerebellum but Its Deficiency Does Not Affect the Development of This Tissue

Given the milder phenotype of Vav3-deficient mice, we decided to investigate the possible expression of other Vav family members by RT-PCR using cerebella of different developmental stages. In contrast to the data available at the Allen Brain Atlas, our studies revealed that *Vav2* transcripts are present in this tissue (Figure 7A). The absence of a functional *Vav3* gene did not result in major alterations in the expression levels of the *Vav2* mRNA (Figure 7A). The analysis of *Vav2*$^{-/-}$ mice did not reveal any problems in the overall structure and cytoarchitecture of the cerebellum (Figure 7B), Purkinje cell development, migration and dendritogenesis (Figure 7C), thickness of the molecular cell layer (Figure 7C; data not shown), and numbers of granule cells at the P6 IGL (Figure 7D). The only difference observed was a small increase in the number of granule cells in lobules VI–VII (Figure 7D). We did not observe either differences in the thickness of the EGL between P8 wild-type and Vav2-deficient mice (data not shown). These results indicate that Vav3 is the Vav family member that, per se, has more direct effects in the cerebellum.

Vav3-deficient Mice Show Problems in Motor Coordination and Gaiting

Because the major role of the cerebellum is to ensure motor coordination, we finally determined whether the absence of Vav3 could affect these functions in mice. To this end, we first compared the coordinated motor performance of wild-type and Vav3 mutant mice of different ages using the Rotarod accelerating test. These experiments indicated that

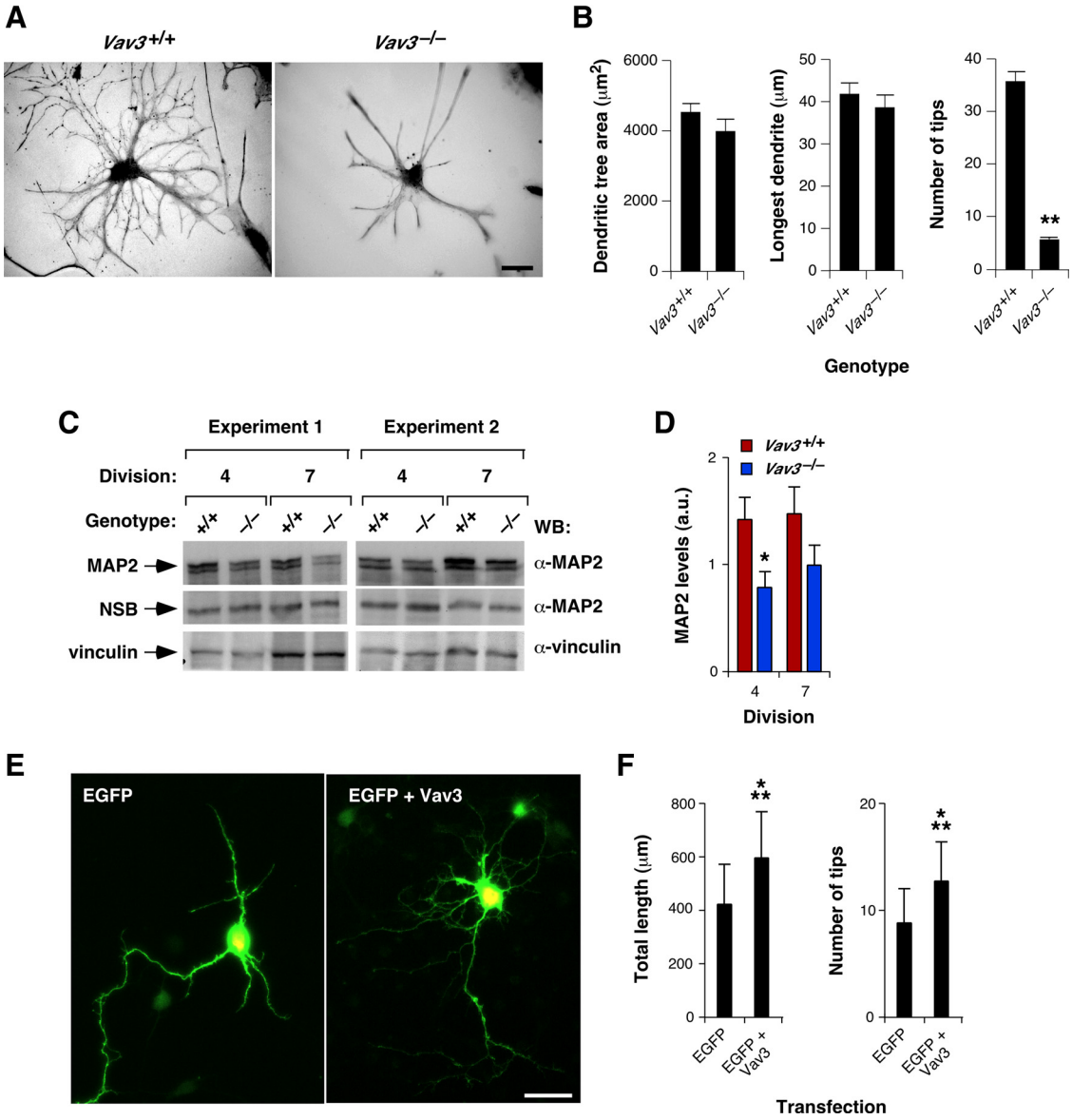

Figure 6. Vav3 regulates dendritic outgrowth in Purkinje and granular cells. (A) Examples of the morphology of Purkinje cells obtained in mixed cultures derived from wild-type mice (left) and Vav3-deficient mice (right). To obtain these images, cell cultures were fixed, stained with anti-calbindin antibodies, and subjected to microscopy analysis. Less dendritic arborization is apparent in cultures generated from *Vav3*$^{-/-}$ mice. (B) Quantification of the Purkinje cell morphology in cultures derived from cerebella of the indicated genotypes. Quantification included the total dendritic tree area (left), the length of the longest dendrite (middle), and the number of branching points (right) in Purkinje cells (n = 4 independent experiments). **$p < 0.01$ compared with wild-type controls. A reduced number of tips is observed in Vav3-deficient Purkinje cells (right). No statistically significant differences were observed in the other two parameters evaluated in these experiments. (C) Expression levels of MAP2 in cultures of granule cell cultures of the indicated genotypes (top). At the indicated divisions in vitro (DIV, top), cellular lysates were obtained, electrophoretically fractionated in 6% SDS-PAGE gels, transferred onto nitrocellulose, and MAP2 levels were determined by anti-MAP2 Western blot (WB) analysis (top). Equal loading was demonstrated by the detection of a nonspecific band recognized by the anti-MAP2 antibody (middle) and by reblotting with an anti-vinculin antibody (bottom). (D) Quantification of MAP2 protein expression in granular cell cultures. Bands from the anti-MAP2 immunoblots obtained in three independent experiments were quantified by densitometry analysis and statistically analyzed. Data are presented as mean and SEM and were normalized taking into consideration the protein levels of vinculin detected in each sample. *$p < 0.05$ compared with wild-type controls. Reduced numbers of MAP2 are seen in cultures from Vav3-deficient mice. (E) Example of wild-type granule cells expressing EGFP alone (left l) or in combination with wild-type Vav3 (right). Cells were processed and transfected as indicated in *Materials and Methods*, fixed at division 4, and photographed using an inverted fluorescence microscope. Bar, 30 μm. Increased dendrite ramifications are seen in the granular cell expressing the Vav3 protein. (F) Quantitation of the total dendritic length (left) and the number of tips (right) of granular cells that were transfected with plasmids encoding the indicated proteins (n = 50 independent cells in each transfection). ***$p < 0.001$ compared with wild-type controls. Vav3 overexpression promotes an increase in the total length and number of tips in the transfected cells.

5-wk-old *Vav3*$^{-/-}$ mice had a markedly impaired performance on a five trail-Rotarod test compared with wild-type littermates (Figure 8A and Supplemental Video S1). Furthermore, when we performed gait analyses, we found that the

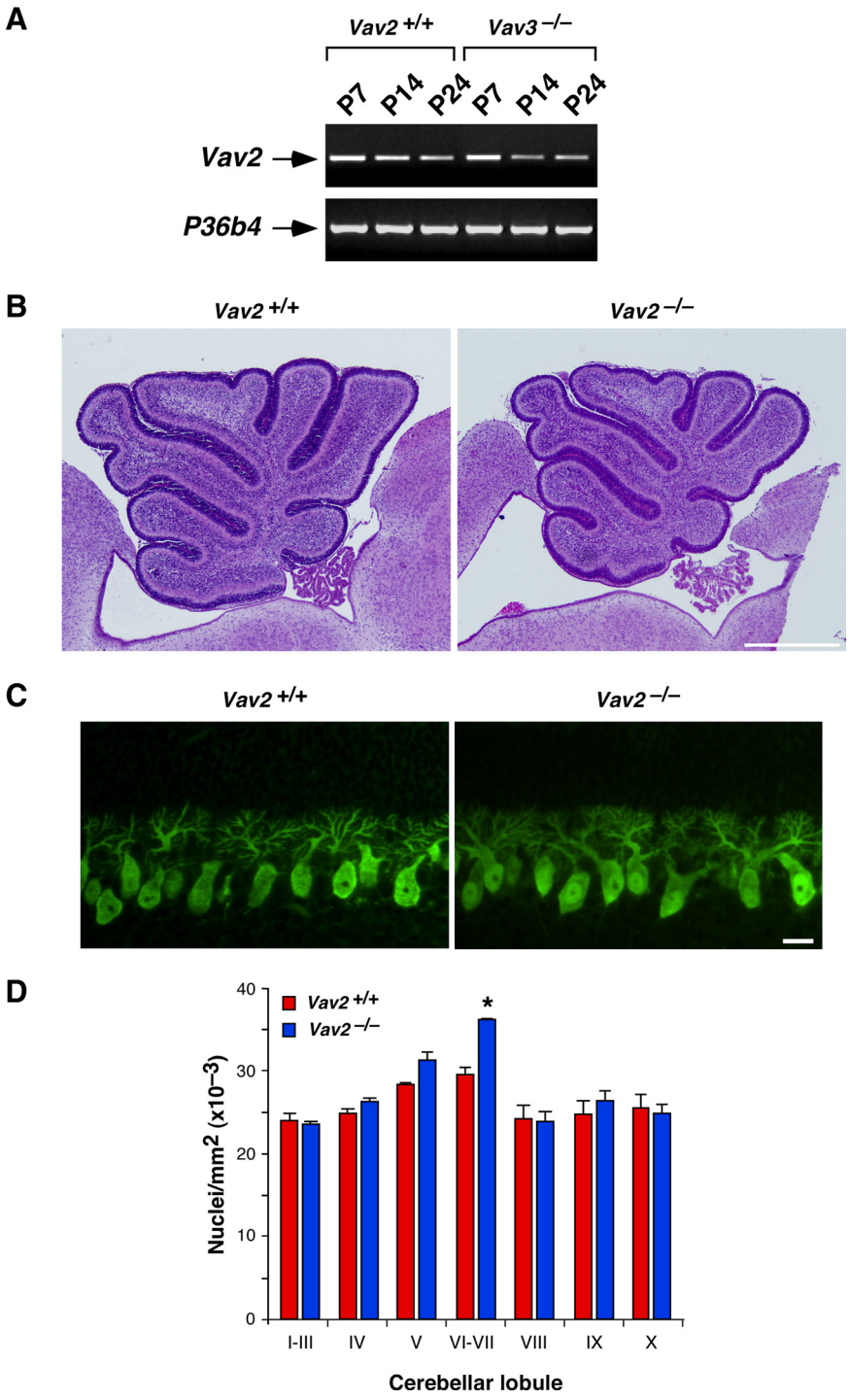

Figure 7. Cerebellar structure of Vav2-deficient mice. (A) Total RNAs obtained from the cerebella of wild-type mice and *Vav3*$^{-/-}$ mice at the indicated P stages were subjected to RT-PCR analysis using oligonucleotide primers for the mouse *Vav2* (top) and *P36b4* (bottom) cDNAs. Final PCR products were separated electrophoretically in agarose gels and photographed. The figure shows the expression of *Vav2* mRNA in all cerebellar stages analyzed and that such expression is not affected by the *Vav3* gene deficiency. (B) Sagittal cerebellar sections from P6 wild-type animals (left) and P6 Vav2-deficient animals (right) were stained with hematoxylin–eosin and analyzed by light microscopy. Bar, 500 μm. No major alterations in cerebellar structure or lobulation are seen in Vav2-deficient mice. (C) Sagittal cerebellar slices from P6 wild-type mice (left) and *Vav2*$^{-/-}$ mice (right) mice subjected to immunostaining with anti-calbindin antibodies and visualized by immunofluorescence microscopy. Bar, 500 μm. No major alterations in Purkinje cell number or dendritogenesis are observed in Vav2-deficient mice. (D) Quantification of the cell density (measured as number of nuclei per square millimeter) present in the IGL of the indicated cerebellar lobules of P6 wild-type mice (red bars) and Vav2-deficient mice (blue bars). The histogram shows the mean and the SEM obtained in each cerebellar lobule using experimental data from three different animals and two independent litters per genotype. *$p < 0.05$ compared with wild-type controls.

distance between strides, the stride length, and the linear axis of the mouse movements were similar between the two groups of animals. However, the normal pattern of hind/fore paw overlap present in wild-type animals was markedly dysfunctional in Vav3-deficient mice (Figure 8, C, E, and F). These defects were significantly ameliorated (in motor coordination problems; Figure 8B) or totally corrected (in the hind/fore paw overlap; Figure 8, D–F) in older, 4-old-mo-old mutant mice. Thus, *Vav3*$^{-/-}$ mice show motor coordination problems that are consistent with cerebellar dysfunction during the first weeks of life.

DISCUSSION

Despite the recognized implication of Rho/Rac proteins and its regulators in a large variety of neuronal functions (Van Aelst and Cline, 2004; Govek *et al*., 2005; Newey *et al*., 2005), very little information has been gathered so far about the function of those proteins in the cerebellum using genetic techniques. For example, although the role of constitutively Rac1 has been studied using transgenic mice in Purkinje cells (Luo *et al*., 1996), the functions of the endogenous Rac1, RhoA, and Cdc42 GTPases could not be addressed in this

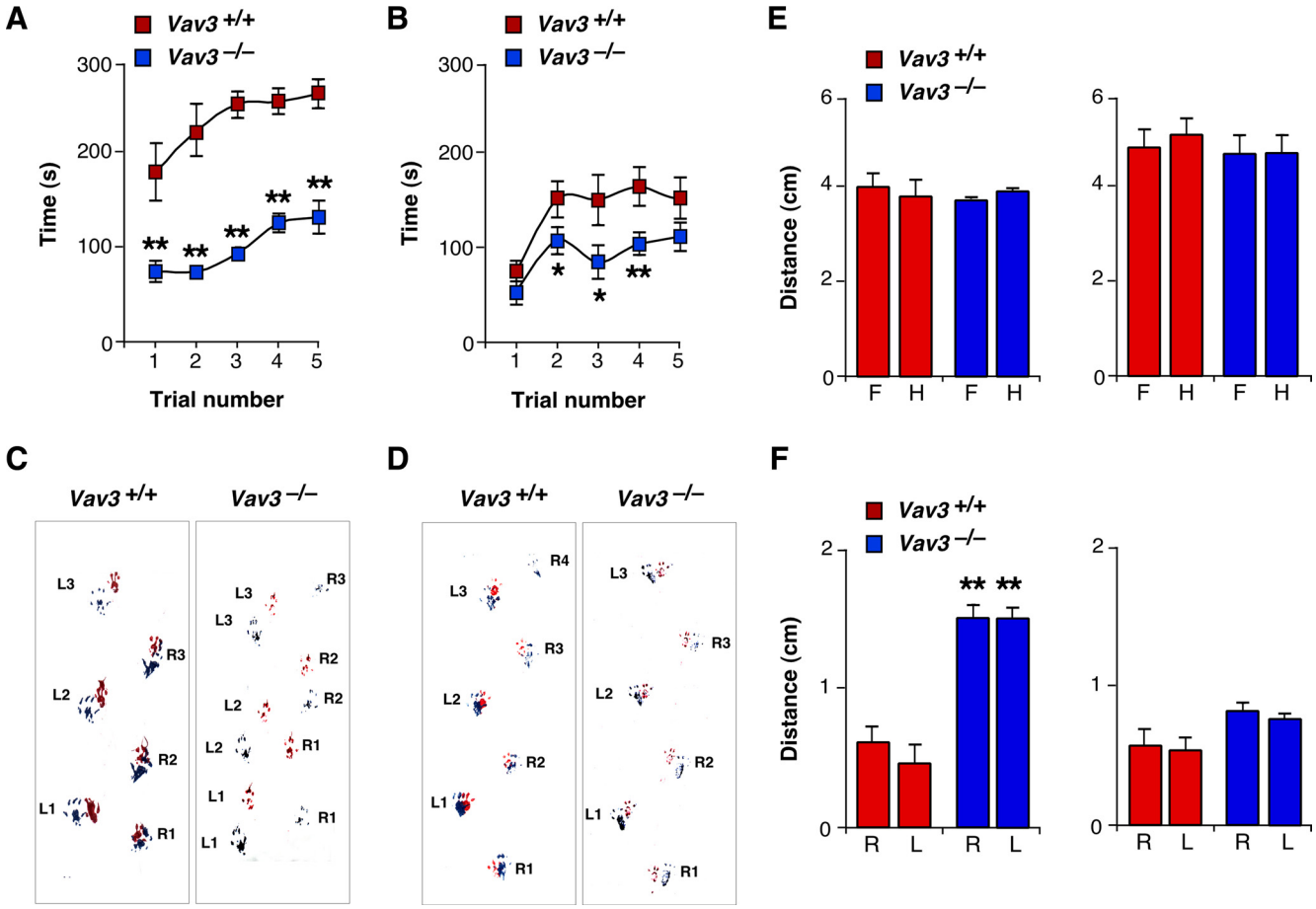

Figure 8. Age-dependent motor coordination problems in Vav3-deficient mice. (A and B) Performance obtained by 5-wk-old (A) and 4-mo-old (red squares) wild-type mice and Vav3-deficient mice (blue squares) during standardized accelerating Rotarod tests (n = 7–9). *p < 0.05 and **p < 0.01 compared with wild-type controls. (C and D) Representative gait analysis of 5-wk-old (C) and 4-mo-old (D) wild-type mice and Vav3-deficient mice ascending an inclined plane. Front and hind paws were painted in red and blue, respectively. (E and F) Quantification of the results obtained in the gait analysis. The distance done by front (F) and hind (H) paws (E) and the distance between the left (L) and right paws (R) of the same side (F) were measured for animals of the indicated genotypes (n = 7–10). Values obtained with 5-wk- and 4-mo-old mice are shown (left and right, respectively). Values derived using wild-type and knockout mice are shown in red and blue bars in the histograms, respectively. The major coordination defects are observed in 5-wk-old Vav3-deficient mice. *p < 0.05 and **p < 0.01 compared with wild-type controls.

tissue as yet due to the embryonic lethality of the respective knockout animals. An important step toward the characterization of Rho/Rac-dependent pathways in this tissue has been the recent report on the phenotype of mice deficient in P-Rex2 and P-Rex1 (Donald *et al.*, 2008), two PIP_3-dependent Rac1 GEFs that are expressed in Purkinje cells in the cerebellum as well as in many other tissues (Welch *et al.*, 2002; Donald *et al.*, 2004, 2008). *P-Rex2*$^{-/-}$ and *P-Rex1*$^{-/-}$;*P-Rex2*$^{-/-}$ mice display very thin primary dendritic stems and motor coordination problems, although they have no apparent defects in the dendritic arborization of Purkinje cells, in other cerebellar cells, or in the overall cerebellar cytoarchitecture (Donald *et al.*, 2008). Although minor, these defects lead to progressive motor coordination and gaiting problems as the mice age (Donald *et al.*, 2008). In this work, we have shown the implication of another Rho/Rac GEF, Vav3, in the cerebellum. Thus, we have demonstrated that the Vav3 deficiency retards specific developmental steps of Purkinje and granule cells and alters the normal formation of the intercrural fissure of the cerebellum. These defects are functionally important, as demonstrated by the severe, age-dependent motor coordination and gaiting defects observed in young *Vav3*$^{-/-}$ mice. Using primary cultures, we have also shown that Vav3 is important for the branching of dendrites in both Purkinje and granule cells. Instead, our in vivo experiments suggest that Vav3 function is dispensable for the formation of spines and axons of cell lines Purkinje cells. This is in contrast with previous reports demonstrating the implication of Vav family members and constitutively active Rac1 in axon guidance events in retina neurons and in Purkinje cell spinogenesis, respectively (Luo *et al.*, 1996; Cowan *et al.*, 2005). Mouse deficient in P-Rex proteins show no defects either in Purkinje cell axogenesis and spinogenesis (Donald *et al.*, 2008), suggesting that other Rho/Rac GEFs are in charge of those biological processes or, alternatively, that the function of Vav3 and/or P-Rex proteins in these biological settings is redundant with the parallel action of other Rho/Rac GEFs. A potential candidate is Tiam1, because this Rac1-specific GEF has been linked to spinogenesis in hippocampal neurons (Zhang and Macara, 2006). Interestingly, *Vav2*$^{-/-}$-deficient mice do not show any significant defects in the developing cerebellum, indicating that the aforementioned functions will not be determined by this exchange factor per se. At this moment, however, we cannot

exclude the possibility that Vav2 and Vav3, or Vav3 and P-Rex proteins, act coordinately in the cerebellum. The future analysis of *Vav2*$^{-/-}$;*Vav3*$^{-/-}$ and *Vav3*$^{-/-}$;*P-Rex*$^{-/-}$ knockout mice will allow to answer this lingering question.

Because Vav3 is expressed in both Purkinje and granule cells, the defects found in Vav3-deficient mice can derive from intrinsic dysfunctions in Purkinje cells, in granule cells or in both cell types. It is also possible that the developmental delays found in the cerebella of those mice could be a manifestation, at least in part, of other underlying biological dysfunctions such as, for example, the establishment of defective, Vav3-dependent intercellular contacts among themselves or with other cell types. The observation that Vav3-deficient Purkinje cells display problems in dendritic arborization but not in spine formation is in agreement with the latter functional scenario because, according to the current model of Purkinje cell development (Sotelo, 2004), the formation of dendrites and spines in this cell type relies on noncell (interactions with other cerebellar neurons) and cell autonomous processes, respectively. This could be also the case of the observed defects in granule cells, for the development and survival of these cells have been shown to rely on proper contacts and cross-talk with Purkinje cells (Sotelo, 2004). The distinction of the cell- and noncell autonomous contributions to the defects found in the cerebella of Vav3-deficient mice will require the generation in the future of Purkinje cell- and granule cell-specific *Vav3* knockout animals.

The *Vav3*$^{-/-}$ mice phenotype resembles, although is not identical to, those found in knockout animals deficient in BDNF, NT3, and calcyphosine 2 (Segal *et al*., 1995; Schwartz *et al*., 1997; Sadakata *et al*., 2007). BDNF and NT3 are ligands for TrkB (Huang and Reichardt, 2003), whereas calcyphosine 2 is a protein involved in secretion of those neurotrophins and thereby contributes to local neurotrophin bioavailability within the cerebellum (Sadakata *et al*., 2004). Such similarity suggests that at least some of the defects found in Vav3-deficient mice could entail the defective activation of the neurotrophin/TrkB signaling axis. Consistent with this possibility, we have found using immunofluorescence studies that the activation of TrkB was severely impaired in EGL granule cells at the P10 stage, an effect that correlates in time with the transient defects observed in the migration of those cells toward the IGL. This defect, however, does not seem to be cell autonomous, because cultures of primary *Vav3*$^{-/-}$ granule cells produce normal levels of BDNF upon stimulation with several stimuli and, in addition, respond to BDNF stimulation with normal levels and kinetics of phosphorylation of TrkB, Erk and Akt. Thus, this activation defects seem to be more related with reduced local availability of TrkB ligands in the EGL at this or immediately prior developmental stages of the cerebellum. It has been shown recently that BDNF regulates the migration of granule cells from the EGL to the IGL through two coordinated mechanisms. On the one hand, BDNF stimulates the motility of granule cells by forming a decreasing gradient from the IGL to EGL. On the other hand, it favors the additional BDNF production by the migrating cell themselves, a process that promotes directionality of the cell movement during the chemotactic process via the localized accumulation of TrkB-containing signaling endosomes at the side of cells where BDNF levels are maximal (Zhou *et al*., 2007). Taking into consideration this functional scenario, together with our present data indicating that primary *Vav3*$^{-/-}$ granule cells produce normal levels of BDNF, we surmise that the deficient migration of P10 EGL cells in Vav3-deficient mice is due to the formation of a weak gradient rather than caused by defects in BDNF production or BDNF signaling responses of the migrating cells. A potential cause of those gradient defects is the reduced numbers of granule cells observed at the P6 stage that could limit the total amount of BDNF produced before the P10 stage. Consistent with this hypothesis, we have observed that the cerebella of P10 *Vav3*$^{-/-}$ mice have a slightly lower BDNF content than those obtained from their wild-type counterparts.

Although it has been shown before that Vav2 and Vav3 act downstream of the nerve growth factor TrkA (Aoki *et al*., 2005), our data do not support the concept that the defects observed in the cerebellum of Vav3-deficient mice are due to the participation of Vav3 in direct TrkB downstream signaling responses. For example, we could not detect any physical interaction between Vav3 and BDNF-stimulated TrkB receptors even when overexpression systems were used. Likewise, BDNF did not induce any detectable phosphorylation of Vav3 on tyrosine residues, a posttranslational modification that is critical for the activation of its Rac1 exchange activity. In contrast, and as described previously (Movilla and Bustelo, 1999; Moores *et al*., 2000; Zeng *et al*., 2000), we have observed that Vav3 does associate with and becomes phosphorylated by other receptors such as the epidermal growth factor (Quevedo and Bustelo, data not shown). Thus, we consider that the phenotypic similarity between Vav3-deficient mice and animals deficient in the neurotrophin/TrkB axis is not a consequence of an implication of Vav3 in downstream TrkB-dependent routes. This raises in turn the question of the nature of the upstream activator/s of Vav3 in cerebellar neurons. These cells express, in addition to Trk family kinases, a large number of tyrosine kinase-linked membrane receptors (c-Met, EGF-R/ErbB1, ErbB4, ErbB3, EphB2, FGF-R, chemokine receptors, insulin receptor family members, integrins, and cell adhesion molecules), many of which have been shown to activate Vav proteins in other cell contexts via intrinsic kinase domains or associated cytoplasmic tyrosine kinases (Bustelo, 2000, 2008; Bustelo, 2000, 2008; Bustelo and Couceiro, 2008). It is possible therefore that some of those molecules could be in charge of the activation of Vav3 in cerebellar neurons. The elucidation of this question will contribute to a better understanding of the biological processes that condition the development, cytoarchitecture, and functional status of the cerebellum in postembryonic stages.

Despite the cerebellar defects found in P-Rex– and Vav3-deficient mice, it is likely that the activation of Rac1 and Rho/Rac proteins in the cerebellum is not limited to the use of these Rho/Rac GEFs. Indeed, the Allen Brain Atlas records the presence of at least 18 additional Rho/Rac GEFs in cerebellar granular and/or Purkinje cell layers, a feature that adds further complexity and plasticity to the mechanisms by which cerebellar cells can induce the activation of these GTPases. It will be important to generate in the future cerebellum-specific knockouts for Rho/Rac GTPases and GEFs to obtain a comprehensive view of the role of each of those proteins in the development and function of the cerebellum.

ACKNOWLEDGMENTS

We thank Maite Blázquez, Javier Tamame and Teresa Iglesias for technical help. We also thank Drs. Beatriz Rico and Constantino Sotelo for helpful comments on the manuscript. X.R.B. work is supported by grants from the National Institutes of Health (5R01-CA73735-13), the Spanish Ministry of Science and Innovation (SMSI) (SAF2006-01789), the Red Temática de Investigación Cooperativa en Cáncer (RD06/0020/0001), and the Castilla y León Autonomous Government (SA053A05 and GR97). C. Q. and M.M.M. were supported by the Red Temática de Investigación Cooperativa en Cáncer. V. S. was partially supported by an SMSI Juan de la Cierva postdoctoral contract and, currently, by an SMSI Ramon y Cajal contract associated to the Consejo Superior de Investigaciones Cientificas. A.C.C. was supported by an SMSI

Formación de Personal Universitano predoctoral fellowship and, currently, by the Red Temática de Investigación Cooperativa en Cáncer. X.R.B.'s laboratory has been recognized as a Consolidated Cancer Research Group by the Asociación Española contra el Cáncer. The activities of the Centro de Investigación del Cáncer are partially supported by the Ramón Areces Foundation and by the Foundation for Cancer Research at the University of Salamanca.

REFERENCES

Adams, N. C., Tomoda, T., Cooper, M., Dietz, G., and Hatten, M. E. (2002). Mice that lack astrotactin have slowed neuronal migration. Development *129*, 965–972.

Aghazadeh, B., Lowry, W. E., Huang, X. Y., and Rosen, M. K. (2000). Structural basis for relief of autoinhibition of the Dbl homology domain of proto-oncogene Vav by tyrosine phosphorylation. Cell *102*, 625–633.

Altman, J. (1972a). Postnatal development of the cerebellar cortex in the rat. I. The external germinal layer and the transitional molecular layer. J. Comp. Neurol. *145*, 353–397.

Altman, J. (1972b). Postnatal development of the cerebellar cortex in the rat. II. Phases in the maturation of Purkinje cells and of the molecular layer. J. Comp. Neurol. *145*, 399–463.

Altman, J. (1972c). Postnatal development of the cerebellar cortex in the rat. III. Maturation of the components of the granular layer. J. Comp. Neurol. *145*, 465–513.

Aoki, K., Nakamura, T., Fujikawa, K., and Matsuda, M. (2005). Local phosphatidylinositol 3,4,5-trisphosphate accumulation recruits Vav2 and Vav3 to activate Rac1/Cdc42 and initiate neurite outgrowth in nerve growth factor-stimulated PC12 cells. Mol. Biol. Cell *16*, 2207–2217.

Buckley, K. M. (1994). Molecular analysis of a secretory organelle: structure and function of synaptic vesicle-specific proteins. J. Membr. Biol. *139*, 75–80.

Bustelo, X. R. (2000). Regulatory and signaling properties of the Vav family. Mol. Cell. Biol. *20*, 1461–1477.

Bustelo, X. R. (2001). Vav proteins, adaptors and cell signaling. Oncogene *20*, 6372–6381.

Bustelo, X. R. (2008). Vav2. UCSD Nature Mol Pages (doi: 10.1038/mp.a002361.002301).

Bustelo, X. R., and Couceiro, J. R. (2008). Vav3. UCSD Nature Mol Pages (doi: 10.1038/mp.a002362.002301).

Bustelo, X. R., Sauzeau, V., and Berenjeno, I. M. (2007). GTP-binding proteins of the Rho/Rac family: regulation, effectors and functions *in vivo*. Bioessays *29*, 356–370.

Cella, M., Fujikawa, K., Tassi, I., Kim, S., Latinis, K., Nishi, S., Yokoyama, W., Colonna, M., and Swat, W. (2004). Differential requirements for Vav proteins in DAP10- and ITAM-mediated NK cell cytotoxicity. J. Exp. Med. *200*, 817–823.

Chen, Y. T., Collins, L. L., Uno, H., and Chang, C. (2005). Deficits in motor coordination with aberrant cerebellar development in mice lacking testicular orphan nuclear receptor 4. Mol. Cell. Biol. *25*, 2722–2732.

Christakos, S., Rhoten, W. B., and Feldman, S. C. (1987). Rat calbindin D28K: purification, quantitation, immunocytochemical localization, and comparative aspects. Methods Enzymol. *139*, 534–551.

Couceiro, J. R., Martin-Bermudo, M. D., and Bustelo, X. R. (2005). Phylogenetic conservation of the regulatory and functional properties of the Vav oncoprotein family. Exp. Cell Res. *308*, 364–380.

Cowan, C. W., Shao, Y. R., Sahin, M., Shamah, S. M., Lin, M. Z., Greer, P. L., Gao, S., Griffith, E. C., Brugge, J. S., and Greenberg, M. E. (2005). Vav family GEFs link activated Ephs to endocytosis and axon guidance. Neuron *46*, 205–217.

Crespo, P., Schuebel, K. E., Ostrom, A. A., Gutkind, J. S., and Bustelo, X. R. (1997). Phosphotyrosine-dependent activation of Rac-1 GDP/GTP exchange by the vav proto-oncogene product. Nature *385*, 169–172.

Donald, S., *et al*. (2004). P-Rex2, a new guanine-nucleotide exchange factor for Rac. FEBS Lett. *572*, 172–176.

Donald, S., Humby, T., Fyfe, I., Segonds-Pichon, A., Walker, S. A., Andrews, S. R., Coadwell, W. J., Emson, P., Wilkinson, L. S., and Welch, H. C. (2008). P-Rex2 regulates Purkinje cell dendrite morphology and motor coordination. Proc. Natl. Acad. Sci. USA *105*, 4483–4488.

Doody, G. M., Bell, S. E., Vigorito, E., Clayton, E., McAdam, S., Tooze, R., Fernandez, C., Lee, I. J., and Turner, M. (2001). Signal transduction through Vav-2 participates in humoral immune responses and B cell maturation. Nat. Immunol. *2*, 542–547.

Doody, G. M., Billadeau, D. D., Clayton, E., Hutchings, A., Berland, R., McAdam, S., Leibson, P. J., and Turner, M. (2000). Vav-2 controls NFAT-dependent transcription in B- but not T-lymphocytes. EMBO J. *19*, 6173–6184.

Etienne-Manneville, S., and Hall, A. (2002). Rho GTPases in cell biology. Nature *420*, 629–635.

Faccio, R., Teitelbaum, S. L., Fujikawa, K., Chappel, J., Zallone, A., Tybulewicz, V. L., Ross, F. P., and Swat, W. (2005). Vav3 regulates osteoclast function and bone mass. Nat. Med. *11*, 284–290.

Friedrich, P., and Aszodi, A. (1991). MAP *2*, a sensitive cross-linker and adjustable spacer in dendritic architecture. FEBS Lett. *295*, 5–9.

Fujikawa, K., *et al*. (2003). Vav1/2/3-null mice define an essential role for Vav family proteins in lymphocyte development and activation but a differential requirement in MAPK signaling in T and B cells. J. Exp. Med. *198*, 1595–1608.

Gakidis, M. A., Cullere, X., Olson, T., Wilsbacher, J. L., Zhang, B., Moores, S. L., Ley, K., Swat, W., Mayadas, T., and Brugge, J. S. (2004). Vav GEFs are required for beta2 integrin-dependent functions of neutrophils. J. Cell Biol. *166*, 273–282.

Govek, E. E., Newey, S. E., and Van Aelst, L. (2005). The role of the Rho GTPases in neuronal development. Genes Dev. *19*, 1–49.

Hall, A. B., Gakidis, M. A., Glogauer, M., Wilsbacher, J. L., Gao, S., Swat, W., and Brugge, J. S. (2006). Requirements for Vav guanine nucleotide exchange factors and Rho GTPases in FcgammaR- and complement-mediated phagocytosis. Immunity *24*, 305–316.

Hatten, M. E., and Heintz, N. (1995). Mechanisms of neural patterning and specification in the developing cerebellum. Annu. Rev. Neurosci. *18*, 385–408.

Huang, E. J., and Reichardt, L. F. (2003). Trk receptors: roles in neuronal signal transduction. Annu. Rev. Biochem. *72*, 609–642.

Hunter, S. G., Zhuang, G., Brantley-Sieders, D., Swat, W., Cowan, C. W., and Chen, J. (2006). Essential role of Vav family guanine nucleotide exchange factors in EphA receptor-mediated angiogenesis. Mol. Cell. Biol. *26*, 4830–4842.

Krueger, B. K., Burne, J. F., and Raff, M. C. (1995). Evidence for large-scale astrocyte death in the developing cerebellum. J. Neurosci. *15*, 3366–3374.

Llorca, O., Arias-Palomo, E., Zugaza, J. L., and Bustelo, X. R. (2005). Global conformational rearrangements during the activation of the GDP/GTP exchange factor Vav3. EMBO J. *24*, 1330–1340.

Luo, L., Hensch, T. K., Ackerman, L., Barbel, S., Jan, L. Y., and Jan, Y. N. (1996). Differential effects of the Rac GTPase on Purkinje cell axons and dendritic trunks and spines. Nature *379*, 837–840.

Miletic, A. V., Graham, D. B., Montgrain, V., Fujikawa, K., Kloeppel, T., Brim, K., Weaver, B., Schreiber, R., Xavier, R., and Swat, W. (2007). Vav proteins control MyD88-dependent oxidative burst. Blood *109*, 3360–3368.

Moores, S. L., Selfors, L. M., Fredericks, J., Breit, T., Fujikawa, K., Alt, F. W., Brugge, J. S., and Swat, W. (2000). Vav family proteins couple to diverse cell surface receptors. Mol. Cell. Biol. *20*, 6364–6373.

Morara, S., Brecha, N. C., Marcotti, W., Provini, L., and Rosina, A. (1996). Neuronal and glial localization of the GABA transporter GAT-1 in the cerebellar cortex. Neuroreport *7*, 2993–2996.

Movilla, N., and Bustelo, X. R. (1999). Biological and regulatory properties of Vav-3, a new member of the Vav family of oncoproteins. Mol. Cell. Biol. *19*, 7870–7885.

Newey, S. E., Velamoor, V., Govek, E. E., and Van Aelst, L. (2005). Rho GTPases, dendritic structure, and mental retardation. J. Neurobiol. *64*, 58–74.

Pearce, A. C., McCarty, O. J., Calaminus, S. D., Vigorito, E., Turner, M., and Watson, S. P. (2007). Vav family proteins are required for optimal regulation of PLCgamma2 by integrin alphaIIbbeta3. Biochem. J. *401*, 753–761.

Pearce, A. C., Senis, Y. A., Billadeau, D. D., Turner, M., Watson, S. P., and Vigorito, E. (2004). Vav1 and vav3 have critical but redundant roles in mediating platelet activation by collagen. J. Biol. Chem. *279*, 53955–53962.

Rico, B., Xu, B., and Reichardt, L. F. (2002). TrkB receptor signaling is required for establishment of GABAergic synapses in the cerebellum. Nat. Neurosci. *5*, 225–233.

Rocamora, N., Garcia-Ladona, F. J., Palacios, J. M., and Mengod, G. (1993). Differential expression of brain-derived neurotrophic factor, neurotrophin-3, and low-affinity nerve growth factor receptor during the postnatal development of the rat cerebellar system. Brain Res. Mol. Brain Res. *17*, 1–8.

Saab, C. Y., and Willis, W. D. (2003). The cerebellum: organization, functions and its role in nociception. Brain Res. Brain Res Rev. *42*, 85–95.

Sadakata, T., et al. (2007). Impaired cerebellar development and function in mice lacking CAPS2, a protein involved in neurotrophin release. J. Neurosci. *27*, 2472–2482.

Sadakata, T., Mizoguchi, A., Sato, Y., Katoh-Semba, R., Fukuda, M., Mikoshiba, K., and Furuichi, T. (2004). The secretory granule-associated protein CAPS2 regulates neurotrophin release and cell survival. J. Neurosci. *24*, 43–52.

Salman, M. S. (2002). The cerebellum: it's about time! But timing is not everything–new insights into the role of the cerebellum in timing motor and cognitive tasks. J. Child. Neurol. *17*, 1–9.

Sauzeau, V., Jerkic, M., Lopez-Novoa, J. M., and Bustelo, X. R. (2007). Loss of Vav2 proto-oncogene causes tachycardia and cardiovascular disease in mice. Mol. Biol. Cell *18*, 943–952.

Sauzeau, V., Sevilla, M. A., Montro, M. J., and Bustelo, X. R. (2010). The Rho/Rac exchange factor Vav2 controls nitric oxide-dependent responses in vascular smooth muscle cells. J. Clin. Inv. *120*, 315–330.

Sauzeau, V., Sevilla, M. A., Rivas-Elena, J. V., de Alava, E., Montero, M. J., Lopez-Novoa, J. M., and Bustelo, X. R. (2006). Vav3 proto-oncogene deficiency leads to sympathetic hyperactivity and cardiovascular dysfunction. Nat. Med. *12*, 841–845.

Saveliev, A., and Tybulewicz, V. L. (2009). Lymphocyte signaling: beyond knockouts. Nat. Immunol. *10*, 361–364.

Schuebel, K. E., Movilla, N., Rosa, J. L., and Bustelo, X. R. (1998). Phosphorylation-dependent and constitutive activation of Rho proteins by wild-type and oncogenic Vav-2. EMBO J. *17*, 6608–6621.

Schwartz, P. M., Borghesani, P. R., Levy, R. L., Pomeroy, S. L., and Segal, R. A. (1997). Abnormal cerebellar development and foliation in BDNF$-/-$ mice reveals a role for neurotrophins in CNS patterning. Neuron *19*, 269–281.

Segal, R. A., Bhattacharyya, A., Rua, L. A., Alberta, J. A., Stephens, R. M., Kaplan, D. R., and Stiles, C. D. (1996). Differential utilization of Trk autophosphorylation sites. J. Biol. Chem. *271*, 20175–20181.

Segal, R. A., Pomeroy, S. L., and Stiles, C. D. (1995). Axonal growth and fasciculation linked to differential expression of BDNF and NT3 receptors in developing cerebellar granule cells. J. Neurosci. *15*, 4970–4981.

Sotelo, C. (2004). Cellular and genetic regulation of the development of the cerebellar system. Prog. Neurobiol. *72*, 295–339.

Stephens, R. M., Loeb, D. M., Copeland, T. D., Pawson, T., Greene, L. A., and Kaplan, D. R. (1994). Trk receptors use redundant signal transduction pathways involving SHC and PLC-gamma 1 to mediate NGF responses. Neuron *12*, 691–705.

Tartare-Deckert, S., Monthouel, M. N., Charvet, C., Foucault, I., Van Obberghen, E., Bernard, A., Altman, A., and Deckert, M. (2001). Vav2 activates c-fos serum response element and CD69 expression but negatively regulates nuclear factor of activated T cells and interleukin-2 gene activation in T lymphocyte. J. Biol. Chem. *276*, 20849–20857.

Turner, M., and Billadeau, D. D. (2002). VAV proteins as signal integrators for multi-subunit immune-recognition receptors. Nat. Rev. Immunol. *2*, 476–486.

Van Aelst, L., and Cline, H. T. (2004). Rho GTPases and activity-dependent dendrite development. Curr. Opin. Neurobiol. *14*, 297–304.

Wechsler-Reya, R. J., and Scott, M. P. (1999). Control of neuronal precursor proliferation in the cerebellum by Sonic Hedgehog. Neuron *22*, 103–114.

Welch, H. C., Coadwell, W. J., Ellson, C. D., Ferguson, G. J., Andrews, S. R., Erdjument-Bromage, H., Tempst, P., Hawkins, P. T., and Stephens, L. R. (2002). P-Rex1, a PtdIns(3,4,5)P3- and Gbetagamma-regulated guanine-nucleotide exchange factor for Rac. Cell *108*, 809–821.

Wetmore, C., Ernfors, P., Persson, H., and Olson, L. (1990). Localization of brain-derived neurotrophic factor mRNA to neurons in the brain by in situ hybridization. Exp. Neurol. *109*, 141–152.

Wood, K. A., Dipasquale, B., and Youle, R. J. (1993). In situ labeling of granule cells for apoptosis-associated DNA fragmentation reveals different mechanisms of cell loss in developing cerebellum. Neuron *11*, 621–632.

Yamasaki, T., Kawaji, K., Ono, K., Bito, H., Hirano, T., Osumi, N., and Kengaku, M. (2001). Pax6 regulates granule cell polarization during parallel fiber formation in the developing cerebellum. Development *128*, 3133–3144.

Zeng, L., Sachdev, P., Yan, L., Chan, J. L., Trenkle, T., McClelland, M., Welsh, J., and Wang, L. H. (2000). Vav3 mediates receptor protein tyrosine kinase signaling, regulates GTPase activity, modulates cell morphology, and induces cell transformation. Mol. Cell. Biol. *20*, 9212–9224.

Zhang, H., and Macara, I. G. (2006). The polarity protein PAR-3 and TIAM1 cooperate in dendritic spine morphogenesis. Nat. Cell Biol. *8*, 227–237.

Zhou, P., Porcionatto, M., Pilapil, M., Chen, Y., Choi, Y., Tolias, K. F., Bikoff, J. B., Hong, E. J., Greenberg, M. E., and Segal, R. A. (2007). Polarized signaling endosomes coordinate BDNF-induced chemotaxis of cerebellar precursors. Neuron *55*, 53–68.